



Measurements of $\psi(2S)$ and $\chi_{c1}(3872)$ production within fully reconstructed jets

LHCb collaboration[†]

Abstract

This paper presents the first measurement of $\psi(2S)$ and $\chi_{c1}(3872)$ meson production within fully reconstructed jets. Each quarkonium state (tag) is reconstructed via its decay to the $J/\psi(\rightarrow\mu^+\mu^-)\pi^+\pi^-$ final state in the forward region using proton-proton collision data collected by the LHCb experiment at the center-of-mass-energy of 13 TeV in 2016, corresponding to an integrated luminosity of 1.64 fb^{-1} . The fragmentation function, presented as the ratio of the quarkonium-tag transverse momentum to the full jet transverse momentum ($p_T(\text{tag})/p_T(\text{jet})$), is measured differentially in $p_T(\text{jet})$ and $p_T(\text{tag})$ bins. The distributions are separated into promptly produced quarkonia from proton-proton collisions and quarkonia produced from displaced b -hadron decays. While the displaced quarkonia fragmentation functions are in general well described by parton-shower predictions, the prompt quarkonium distributions differ significantly from fixed-order non-relativistic QCD (NRQCD) predictions followed by a QCD parton shower.

Submitted to Eur. Phys. J. C

© 2024 CERN for the benefit of the LHCb collaboration. CC BY 4.0 licence.

[†]Authors are listed at the end of this paper.

1 Introduction

The production of quarkonium states, flavourless mesons composed of at least a c or b quark and its corresponding antiquark, provides a unique probe for studying quantum chromodynamics (QCD) [1]. The masses of the observed quarkonium states, ranging from 3 to 11 GeV/ c^2 , cover the transition between the perturbative and nonperturbative regimes of QCD. In proton-proton (pp) collisions at the LHC, these quarkonium states can be produced at center-of-mass energies which are orders of magnitude larger than their relatively low masses. Consequently, any model attempting to successfully predict the production of quarkonia must span a wide range of energy scales.

Extensive differential cross-section measurements have been performed for the production of the J/ψ meson, the lightest vector quarkonium state, in hadron-hadron collisions at a variety of experiments [2–10] including those at the LHC [11–17]. Production cross-sections for the heavier excited states such as the $\psi(2S)$, $\psi(3770)$, χ_c , Υ , and χ_b resonances have also been measured at the LHC [18–22]. Many of these measurements can be described by nonrelativistic QCD (NRQCD) [23–25], an effective field theory where the production of the quarkonium state is factorized into a perturbative (short-distance) and nonperturbative (long-distance) component.

However, most NRQCD-based calculations for quarkonia production at the Tevatron and LHC [26–34] predict large transverse polarization of the J/ψ and $\psi(2S)$ mesons, which is not observed in data [35–41], with similar results observed at RHIC [42, 43]. Indeed, NRQCD fails to simultaneously describe all measured quarkonium observables [44, 45]. Additionally, fixed-order NRQCD predicts J/ψ mesons to be produced mostly isolated, while jet fragmentation measurements at the LHC demonstrate that J/ψ mesons are predominantly produced surrounded by nearby particles, within jet radii of $R = 0.3$ and $R = 0.5$ [46–48]. Developments in calculating quarkonium fragmentation functions [49, 50] and quarkonium production in parton showers [51] may help resolve these isolation discrepancies observed in jets while also consistently describing other observables.

This incomplete knowledge about quarkonia production mechanisms has wide implications on the study of the medium formed in ultrarelativistic heavy-ion collisions [52]. Indeed, quarkonia not produced from particle decays are commonly expected to form in the very early stages of particle collisions and so they are regularly used as probes of the hot and dense medium created in heavy-ion collisions.

The reconstruction of identified particles within fully reconstructed jets is a unique way to study the underlying mechanisms involved in the production of these particles. Despite these prospects, only a few measurements of jet fragmentation functions of identified particles have been performed. Among them are studies of D^0 [53, 54], $D^{*\pm}$ [55–59] and B^\pm mesons [60], and Λ_c^+ baryons [61]. The production of quarkonia as components of jets remains largely unexplored and provides an important handle on understanding the mechanisms behind quarkonia production in hadron-hadron collisions. To date, measurements have been limited to the J/ψ state only [46, 48]. In this paper, for the first time, measurements of fragmentation functions of $\psi(2S)$ and $\chi_{c1}(3872)$ mesons are presented. Both mesons (referred to as tags from here on) are reconstructed using the $J/\psi(\rightarrow\mu^+\mu^-)\pi^+\pi^-$ decay channel. The fragmentation functions are measured through the transverse momentum ratio $z \equiv p_T(\text{tag})/p_T(\text{jet})$, with p_T the component of the momentum transverse to the beam. The fraction of prompt $\psi(2S)$ states that are produced from feed-down of higher-mass resonances is significantly smaller compared to the J/ψ meson [62],

making it an ideal candidate for the theoretical interpretation of quarkonium formation. These measurements are performed differentially in both the transverse momentum of the quarkonium, $p_{\text{T}}(\text{tag})$, and of the jet, $p_{\text{T}}(\text{jet})$.

2 Detector and dataset

The LHCb detector [63, 64] is a single-arm forward spectrometer covering the pseudorapidity range $2.0 < \eta < 5.0$, designed for the study of particles containing b and c quarks. The detector includes a high-precision tracking system consisting of a silicon-strip vertex detector surrounding the pp interaction region, a large-area silicon-strip detector located upstream of a dipole magnet with a bending power of about 4 T m, and three stations of silicon-strip detectors and straw drift tubes placed downstream of the magnet. The tracking system measures the momentum, p , of charged particles with a relative uncertainty that varies from 0.5% at low momentum to 1.0% at 200 GeV/ c . The minimum distance of a track to a primary pp collision vertex (PV), called the impact parameter (IP), is measured with a resolution of $(15 + 29/p_{\text{T}}) \mu\text{m}$, where p_{T} is in units of GeV/ c . Different types of charged hadrons are distinguished using information from two ring-imaging Cherenkov detectors (RICH). Photons, electrons and hadrons are identified by a calorimeter system consisting of scintillating-pad and preshower detectors, an electromagnetic and a hadronic calorimeter. Muons are identified by a system composed of alternating layers of iron and multiwire proportional chambers [65].

The data sample used in this analysis is collected from pp collisions at a center-of-mass energy of $\sqrt{s} = 13 \text{ TeV}$, and corresponds to an integrated luminosity of 1.64 fb^{-1} recorded during 2016. The online event selection is performed by a trigger [66] that consists of a hardware stage using information from the calorimeter and muon systems, followed by a software stage that performs the $\mu^+\mu^-$ candidate reconstruction. The hardware stage selects events with at least one $\mu^+\mu^-$ candidate with $\sqrt{p_{\text{T}}(\mu^+)p_{\text{T}}(\mu^-)} > 1.3 - 1.5 \text{ GeV}/c$, where the threshold varied during the 2016 data taking period. In the software stage, two oppositely charged muon candidates with $p_{\text{T}}(\mu) > 0.5 \text{ GeV}/c$ are required to form a $\mu^+\mu^-$ candidate with a mass within $\pm 120 \text{ MeV}/c^2$ of the known J/ψ mass [67].

This analysis uses the same data-taking scheme that was first introduced in Ref. [46]. Here, offline-quality track reconstruction [68] is achieved in the online system through real-time alignment and calibration [69]. All fully online reconstructed high-level objects such as particle candidates are retained, while the lower-level detector information is discarded. At the high-level trigger (HLT) stage, this strategy allows the online selection of this analysis to record all events with a $\mu^+\mu^-$ candidate consistent with a J/ψ meson, but with no p_{T} or displacement requirements on the $\mu^+\mu^-$ candidate with respect to the PV.

Simulation is required to model the effects of the detector response and the imposed selection requirements on the $\mu^+\mu^-\pi^+\pi^-$ final state. In the simulation, pp collisions are generated using PYTHIA 8.186 [70] with a specific LHCb configuration [71]. Decays of unstable particles are described by EVTGEN [72], in which final-state radiation is generated using PHOTOS [73]. The interaction of the generated particles with the detector, and its response, are implemented using the GEANT4 toolkit [74] as described in Ref. [75].

3 Event selection

The event selection requires two distinct objects, the quarkonium tag and the jet associated with that tag. Because the tag is a constituent of its associated jet, all possible tags in the event must be selected prior to constructing the jets in the event. Both the $\psi(2S)$ and $\chi_{c1}(3872)$ meson constituents are reconstructed using the $\mu^+\mu^-\pi^+\pi^-$ final state, which is expected to be produced primarily from the intermediate resonance decay $J/\psi \rightarrow \mu^+\mu^-$ in association with two charged pions. The muon and pion candidates are selected from well-reconstructed charged tracks. Tracks matched with hits in the muon stations downstream of the calorimeters that satisfy additional muon-identification criteria from the calorimeters and RICH are identified as muon candidates. Tracks without muon station hits that fulfil pion-identification criteria are taken as charged pion candidates. Both the muon and pion candidates must be reconstructed within the fiducial region of this analysis: their pseudorapidity range is limited to $2.0 < \eta < 4.5$, their transverse momenta to $p_T > 0.5 \text{ GeV}/c$, the momenta of the muons are limited to $p(\mu) > 6 \text{ GeV}/c$, and the momenta of the pions to $p(\pi) > 3 \text{ GeV}/c$.

The $\mu^+\mu^-$ candidates that pass the online criteria should be consistent with a J/ψ meson. Additionally, the two muons originating from the J/ψ candidate must form a good-quality vertex with a distance-of-closest approach (DOCA) between the muon candidates less than 0.2 mm. If the J/ψ candidate is located within $2.0 < \eta(J/\psi) < 4.5$, it is combined with two opposite-sign pion candidates to form a $\psi(2S)$ or $\chi_{c1}(3872)$ tag candidate. The DOCA between the J/ψ candidate and both pion candidates must be less than 0.5 mm. In the first step, tag candidates with a mass $> 4100 \text{ MeV}/c^2$ are discarded from further analysis. For the remaining candidates, the momentum vectors of the four decay particles are fitted, constraining all four tracks to a common vertex and the mass of the $\mu^+\mu^-$ candidate to the known mass of the J/ψ meson [67]. This significantly improves the mass resolution of the tag candidates. If the refitted mass of a tag candidate, $m(\text{tag})$, is $3635 < m(\text{tag}) < 3730 \text{ MeV}/c^2$, the tag is considered to be a $\psi(2S)$ candidate. Alternatively, if the mass is $3830 < m(\text{tag}) < 3920 \text{ MeV}/c^2$ and the decay energy release (Q -value), $Q \equiv m(\mu^+\mu^-\pi^+\pi^-) - m(\mu^+\mu^-) - m(\pi^+\pi^-) < 150 \text{ MeV}/c^2$, the tag is considered a $\chi_{c1}(3872)$ candidate. Requiring this Q -value significantly improves the signal-to-background ratio of the $\chi_{c1}(3872)$ selection [76]. The fiducial volume of the tags is limited to $2.0 < \eta(\text{tag}) < 4.5$ with $p_T(\text{tag}) > 2 \text{ GeV}/c$.

After all possible tag candidates are selected in the event, jets are built using charged and neutral particle candidates, all reconstructed online with the full detector information, using a particle-flow algorithm [77]. The constituent $\mu^+\mu^-\pi^+\pi^-$ tracks of the tag candidates are excluded from this particle-flow input, and instead the tag candidate is considered a single object. If more than one $\mu^+\mu^-\pi^+\pi^-$ combination within the jet radius can form a viable tag candidate, one combination is pseudo-randomly selected and substituted for a single tag object, while the other combinations are left as individual particles in the particle flow for the full jet reconstruction. The anti- k_T sequential clustering algorithm [78] with jet radius parameter $R = 0.5$, as implemented in the FASTJET package [79], is applied to this particle-flow input to produce jets. These jets are required to fall within the fiducial region of $2.5 < \eta(\text{jet}) < 4.0$ with $p_T(\text{jet}) > 5 \text{ GeV}/c$.

For events that contain a jet with one tag constituent, where the tag and the jet fulfil all the selection requirements, a final selection is applied that requires exactly one reconstructed primary vertex per event. Unlike charged particle-flow inputs, neutral

inputs cannot be associated with a primary vertex. By requiring a single vertex, the jet candidate is not contaminated with neutral particle-flow input from other pp interactions. This significantly improves the jet energy resolution and reduces systematic uncertainties arising from modelling the detector response.

4 Signal determination

This analysis relies on the reconstruction of the transverse-momentum fraction of the tag with respect to the jet containing the tag, defined as

$$z \equiv \frac{p_{\text{T}}(\text{tag})}{p_{\text{T}}(\text{jet})}. \quad (1)$$

The distribution of this ratio is measured differentially in intervals of $p_{\text{T}}(\text{tag})$ and $p_{\text{T}}(\text{jet})$, and the distributions are presented separately for tags originating from the primary vertex of the event (prompt) and tags produced from a b -hadron decay (displaced).

The signal yields are determined from unbinned fits to the tag invariant-mass distribution for each z - p_{T} interval, where p_{T} here means either $p_{\text{T}}(\text{tag})$ or $p_{\text{T}}(\text{jet})$. The signal distribution is modelled by the sum of two Crystal Ball (CB) functions [80], which share a common mean and power-law tail exponent, n . The parameter α , which determines the onset of the power-law tail, is fixed to an equal value but with opposite sign for the two CBs. The start values for the α and n parameters are taken from fits to simulation and the uncertainty from these fits are used to limit their parameter ranges. The background distribution is modelled with a first-degree polynomial. The left panels of Figs. 1 and 2 show the full mass range including signal and sideband regions overlaid with sample fits for $\psi(2S)$ and $\chi_{c1}(3872)$ mass distributions in two particular kinematic bins. The signal-to-background ratio increases significantly as z increases, with an almost background-free signal for isolated $\psi(2S)$ and $\chi_{c1}(3872)$ tags.

After performing the mass fits for a given z - p_{T} interval, the prompt and nonprompt signal fractions are determined with an unbinned fit to the pseudo decay-time distribution of the tag,

$$t_z \equiv \lambda \frac{m}{p_z}, \quad (2)$$

where λ is the flight distance projected along the beam axis between the tag decay and primary vertices, m is the nominal mass of the $\psi(2S)$ or $\chi_{c1}(3872)$ meson, and p_z is the component of the tag momentum along the beam axis [14].

For the fit to the t_z distribution the sample is restricted to the $m(\mu^+\mu^-\pi^+\pi^-)$ signal region ($3678 < m(\mu^+\mu^-\pi^+\pi^-) < 3694$ MeV/ c^2 for $\psi(2S)$ and $3860 < m(\mu^+\mu^-\pi^+\pi^-) < 3884$ MeV/ c^2 for $\chi_{c1}(3872)$), to enhance the signal contribution. The background t_z distribution is modelled from the t_z distribution in the mass sideband regions around the known $\psi(2S)$ or $\chi_{c1}(3872)$ meson mass [67], and is fit empirically with a Gaussian core and exponential tails. This distribution is normalized using the background fraction displaced signal distribution with an exponential decay function. Both signal distributions are then convolved with the same double-Gaussian resolution function. The five parameters extracted from the fit are the two Gaussian widths, the ratio contribution from the mass fit. The prompt signal distribution is modelled with a Dirac delta function and the between the two Gaussian normalizations, an exponential

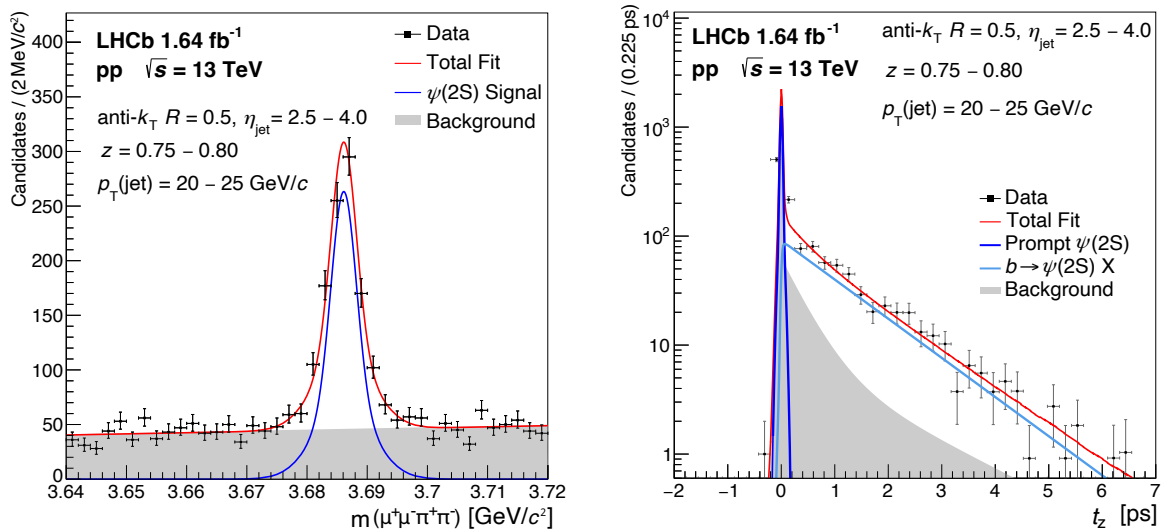


Figure 1: (Left) Invariant-mass distribution and (right) decay-time distribution for $\psi(2S)$ in a single z - $p_T(\text{jet})$ interval at mid z , superimposed with the results from unbinned maximum-likelihood fits. The displaced $\psi(2S)$ fraction in this interval is $(56.4 \pm 2.2)\%$.

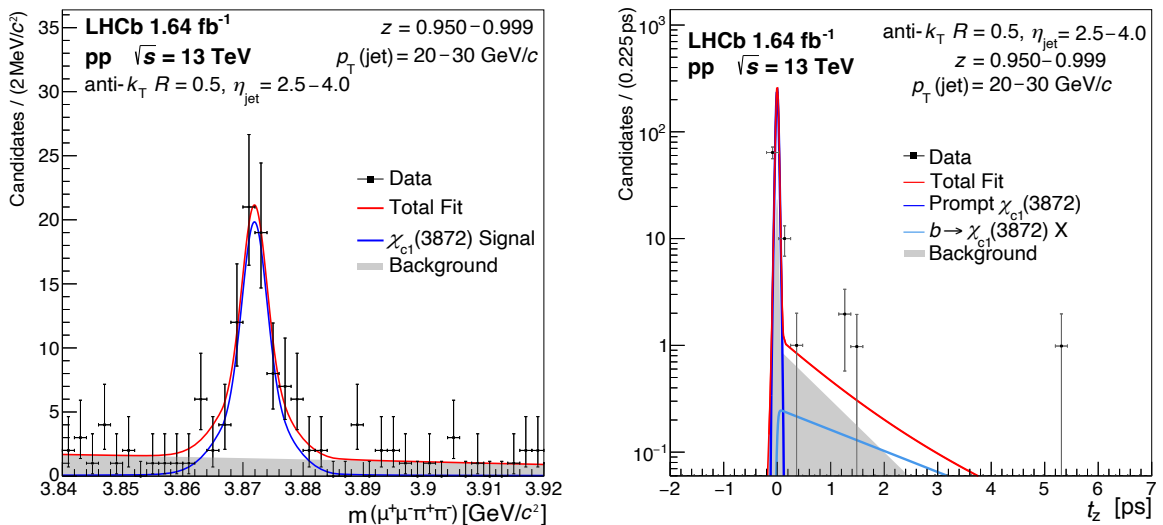


Figure 2: (Left) Invariant-mass distribution and (right) decay-time distribution for $\chi_{c1}(3872)$ in a single z - $p_T(\text{jet})$ interval at high z , superimposed with the results from unbinned maximum-likelihood fits. The displaced $\chi_{c1}(3872)$ fraction in this interval is $(3.5 \pm 2.9)\%$.

decay constant of the displaced signal yield, and the ratio of prompt and displaced signal contributions.

The statistical uncertainties on the signal yields are propagated from the uncertainties of the mass and the t_z fits. The fraction of prompt signal integrated over z is shown in Fig. 3 as a function of the $\psi(2S)$ and $\chi_{c1}(3872)$ p_T , and is consistent with previous LHCb results [19, 81]. The fraction of prompt fragmentation with $z = 1$, which is not part of the

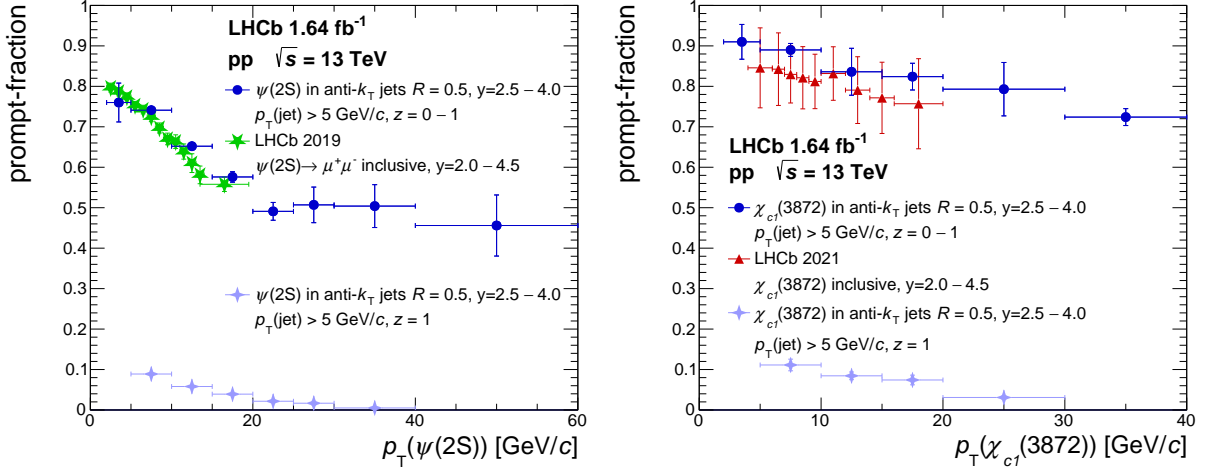


Figure 3: Fraction of prompt (blue circles) signal for (left) $\psi(2S)$ and (right) $\chi_{c1}(3872)$ mesons as a function of their p_T integrated over all z values. The prompt single-particle jets ($z = 1$) which are a subcomponent of the total prompt fraction are displayed separately (violet stars). The results of this analysis are compared to previous LHCb results from 2019 using $\mu^+\mu^-$ final states [19] (green stars) and results from 2021 using $\mu^+\mu^-\pi^+\pi^-$ final states [81] (red triangles), both at $\sqrt{s} = 13$ TeV.

reported fragmentation functions, is shown as well. These single-particle jets comprise only a tiny fraction of the total tag production.

5 Signal efficiencies

The efficiency correction adjusts the signal yield in each z - p_T interval for inefficiencies in the reconstruction and selection procedure of the tag candidates and the jets. The total signal efficiency for the tags is factorized into the product of three efficiencies: online, pion, and tag.

The online efficiency is the efficiency for a $\mu^+\mu^-$ candidate to pass the online reconstruction and selection. The muon reconstruction efficiencies are determined from simulation as a function of $\eta(\mu)$ and $p_T(\mu)$. A tag-and-probe method using data is used to calibrate the simulation to data [82]. The average muon reconstruction efficiency is roughly 95% and is largely independent of the z - p_T interval. The online selection efficiency is determined directly from the data by using an independent set of triggers to those used in this analysis [83]. This efficiency is evaluated as a function of $\eta(\mu^+\mu^-)$ and $\sqrt{p_T(\mu^+)p_T(\mu^-)}$. The online selection efficiency rises with $p_T(\text{jet})$ from roughly 50% for $5 < p_T(\text{jet}) < 8$ GeV/ c , to 75% for $40 < p_T(\text{jet}) < 60$ GeV/ c , and is largely independent of z .

The pion efficiency is the efficiency for a pion to both be reconstructed and pass the analysis selection. The pion reconstruction efficiency is determined using the same method as the muon reconstruction efficiency, but with an additional hadronic-interaction correction derived from control samples. This efficiency increases with $p_T(\text{jet})$ and z , from 50% for $5 < p_T(\text{jet}) < 8$ GeV/ c , to 70% for $40 < p_T(\text{jet}) < 60$ GeV/ c . Simulation is used to determine the pion selection efficiency which corrects for the track-quality

and particle-identification requirements. The efficiency of this selection increases with both z and $p_{\text{T}}(\text{jet})$, from an efficiency of 40% for $5 < p_{\text{T}}(\text{jet}) < 8 \text{ GeV}/c$, to 80% for $40 < p_{\text{T}}(\text{jet}) < 60 \text{ GeV}/c$.

Finally, the tag efficiency is the efficiency for a reconstructed tag to pass either the $\psi(2S)$ or $\chi_{c1}(3872)$ selection requirements. The Q requirement for $\chi_{c1}(3872)$ tags is determined from simulation to be 88% and found to be consistent over all z - p_{T} intervals. The efficiency of DOCA selection between the $\mu^+\mu^-$ and pion candidates is found from simulation to be consistent with 100%.

Since the efficiencies described above are calculated for prompt tag candidates, an additional correction is applied for displaced tag candidates. The decay-time-dependent tracking correction is roughly 105% for tags at intermediate t_z values of $1 < t_z < 5 \text{ ps}$ relative to $t_z = 0 \text{ ps}$. These corrections are applied to the t_z distributions before the t_z fit is performed.

The total efficiency ranges between 8% and 25%, depending on the z - p_{T} interval. In general, the efficiency increases with both $p_{\text{T}}(\text{jet})$ and z . Since the efficiencies are primarily driven by the track reconstruction, when z - $p_{\text{T}}(\text{tag})$ intervals are used, the efficiency is mostly constant over z and increases with $p_{\text{T}}(\text{tag})$ from 5% for $2 < p_{\text{T}}(\text{tag}) < 5 \text{ GeV}/c$, to 28% for $30 < p_{\text{T}}(\text{tag}) < 40 \text{ GeV}/c$.

One final efficiency correction is applied after the unfolding, described in Sec. 6. This is the jet reconstruction efficiency, which corrects for inefficiencies to reconstruct the jet object given that the tag was reconstructed in the detector. The jet reconstruction efficiency is largely constant as a function of z and p_{T} . It falls off for low jet p_{T} (outside the reported ranges) and for large z values close to 1. At large z values the reconstruction efficiencies drop by about 10% to 25% as compared to values at mid- z ranges. The unfolded spectra are corrected for these large- z inefficiencies.

6 Unfolding

Detector resolution effects result in the migration of candidates between z - p_{T} intervals. These migrations are primarily driven by the energy-scale shift and resolution of the $p_{\text{T}}(\text{jet})$, and consequently impact both z and $p_{\text{T}}(\text{jet})$ but not $p_{\text{T}}(\text{tag})$. This analysis applies an iterative unfolding technique [84] based on the ROOUNFOLD package [85]. The detector response matrix maps the generator-level observables to the reconstructed-level observables and is defined using simulation. Current prompt-tag simulations do not provide an adequate description of basic jet properties in the data, such as the slope of the $p_{\text{T}}(\text{jet})$ distribution and the distribution of the number of constituents versus $p_{\text{T}}(\text{jet})$. This leads to insufficient coverage for lower z values. Hence, displaced-tag simulations of $\psi(2S)$ and $\chi_{c1}(3872)$ meson production, which provide better coverage of the data, are used to define the prompt response matrix. The distinction between the displaced and prompt response matrices is primarily driven by the expected difference in the relative fraction of long-lived neutral hadrons which are not reconstructed such as K_{S}^0 mesons and Λ baryons (V^0 s), in these two simulation samples. Samples with larger V^0 fractions result in a downward shift of the jet energy scale. From simulation, the fraction of events with V^0 content is estimated to be 63% in displaced tag production and 28% in prompt tag production. The shift in the jet energy scale for a variety of V^0 fractions, including the expected prompt and displaced fraction, is shown in Fig. 4. The jet energy resolution is

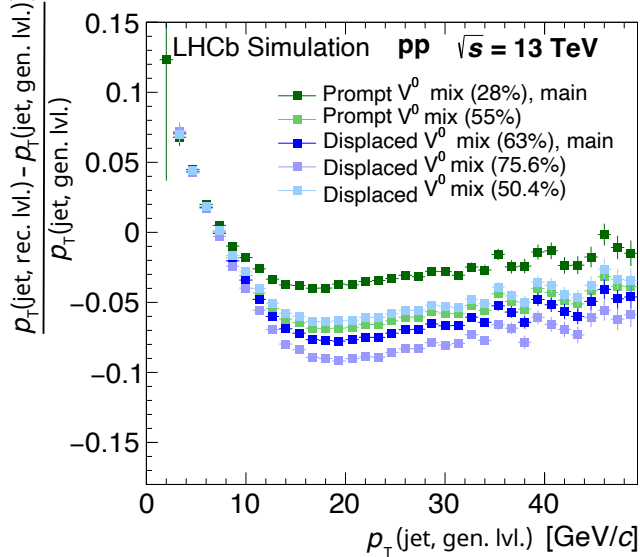


Figure 4: Jet energy scale for different V^0 s fraction variations, including prompt (green) and displaced (blue) variations, as determined from simulation. The percentage of events with V^0 content in these simulations is denoted in brackets. The jet energy scale (JES) is defined as the normalized difference in $p_{\text{T}}(\text{jet})$ retrieved at reconstruction level (rec. lvl.) and at MC generator level (gen. lvl.).

independent of the V^0 fraction and is roughly 15% for $p_{\text{T}}(\text{jet}) = 10 \text{ GeV}/c$ and 13% for $p_{\text{T}}(\text{jet}) = 40 \text{ GeV}/c$.

Both the prompt and displaced response matrices are further corrected to match the data using a momentum-balance technique applied to $Z + \text{jet}$ data [46,77]. Based on these studies the $p_{\text{T}}(\text{jet})$ value is shifted downwards by 4% and the $p_{\text{T}}(\text{jet})$ resolution is increased by 7%. Figure 5 shows the prompt response matrix for the $\psi(2S)$ z - $p_{\text{T}}(\text{jet})$ measurement. Since the measurements of this analysis are doubly differential in z and $p_{\text{T}}(\text{jet})$ or $p_{\text{T}}(\text{tag})$, we apply an iterative two-dimensional Bayesian unfolding procedure until the folding result becomes stable. The lowest measured $p_{\text{T}}(\text{jet})$ interval, $5 < p_{\text{T}}(\text{jet}) < 8 \text{ GeV}/c$, and the lowest measured $p_{\text{T}}(\text{tag})$ interval, $2 < p_{\text{T}}(\text{tag}) < 5 \text{ GeV}/c$, are only used as input for the unfolding to stabilize the output of the second lowest p_{T} interval.

7 Systematic uncertainties

There are two main sources of systematic uncertainties: those from the efficiency determination and those from the unfolding procedure (systematic uncertainties from the signal fits are negligible).

The efficiency uncertainties are fully correlated between z - p_{T} intervals and are determined by varying the efficiency corrections. For the corrections based on simulation, the binning of the muon and pion efficiencies as a function of η and p_{T} is changed. Additionally, the default muon and pion efficiencies are varied within their statistical uncertainties. For the data-driven corrections, the statistical uncertainties are used to vary the efficiencies. For the online (trigger) efficiency, an additional correction is obtained to take into account differences from the true online efficiency to the efficiencies obtained using the independent

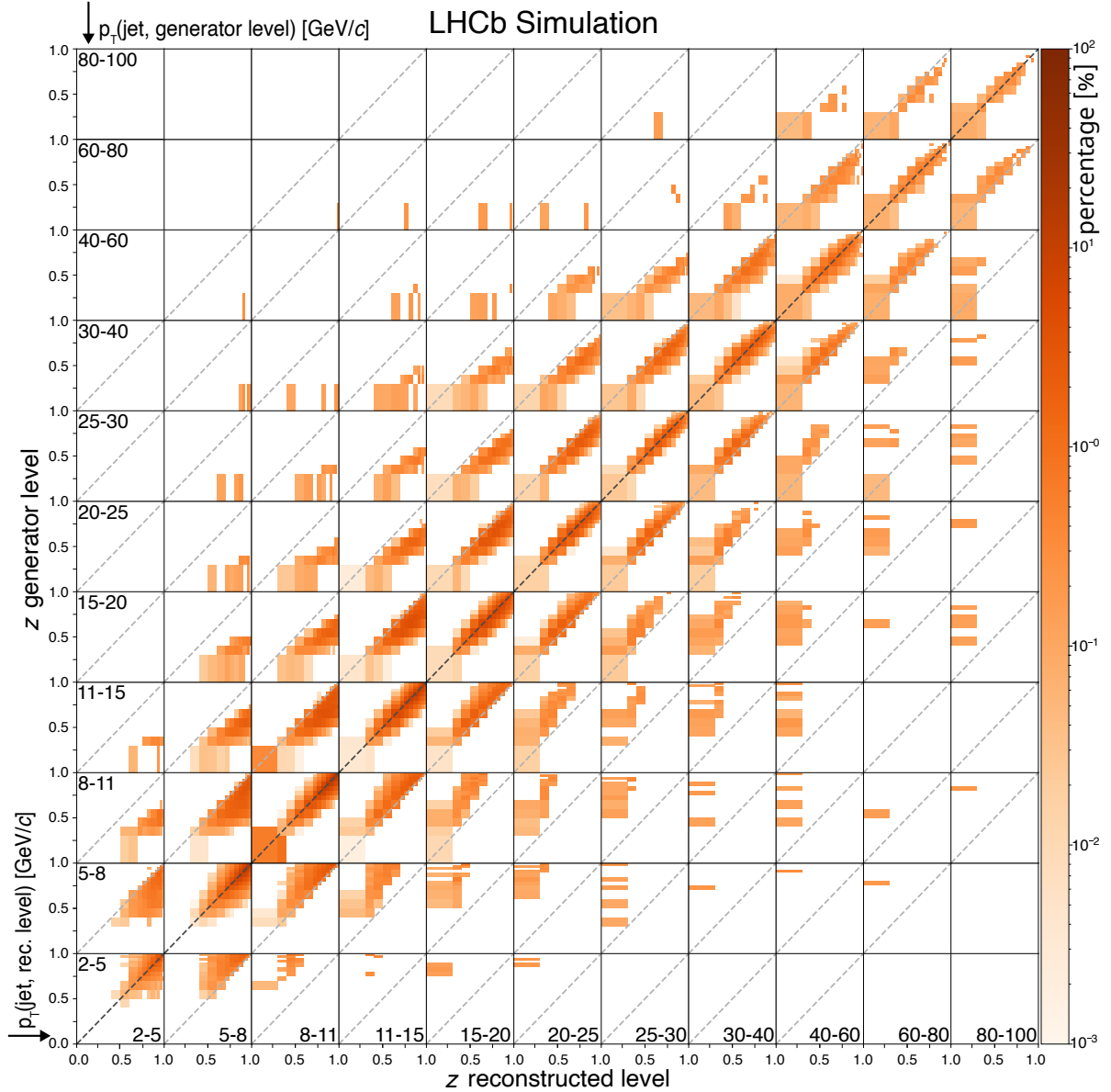


Figure 5: Four-dimensional prompt response matrix for unfolding the $\psi(2S)$ result differential in z and $p_T(\text{jet})$, assuming a percentage of events with V^0 content of 28%. The colour axis represents the bin-to-bin migration probabilities between the generated observable and the reconstructed observable.

set of triggers method in this analysis. The sample used is an inclusive J/ψ sample. The total efficiency uncertainty is the quadratic sum of these contributions and is roughly 6%. This uncertainty is dominated by the variations from the data-driven corrections. For low $p_T(\text{jet})$ and $p_T(\text{tag})$ the efficiency uncertainty increases to $\sim 10\%$ due to the online and pion reconstruction efficiency uncertainties.

The unfolding uncertainties are uncorrelated between z - p_T intervals, and are evaluated by varying the unfolding procedure. They are determined by varying the unfolding regularization parameter and by changing the fraction of V^0 s in the simulation that is used to define the response matrix. Another source of uncertainty arises from the prior

of the generator-level distribution. To evaluate this contribution, three variations are performed. First, a flat prior in z is used. Second, the prompt prior for the displaced response matrix is used and the displaced prior for the prompt response matrix is used. Third, the prior is weighted to match the unfolded result and unfold again with this adapted prior. The unfolding procedure is repeated with all variations and the differences between the results are assigned as systematic uncertainties. Since all variations of the unfolding procedure quantify the same systematic source of uncertainty, the combined uncertainty of the unfolding is calculated by the variance of the differences and is around 10%.

8 Results

This section presents the double-differential z - p_T distributions after the efficiency corrections of Sec. 5 and the unfolding of Sec. 6 are applied. All the provided distributions contain the data together with the uncorrelated statistical uncertainties propagated from the mass and t_z fits (shown as black lines in the figures that follow), the correlated uncertainties due to the efficiency corrections (empty blue boxes) and the uncorrelated uncertainties from the unfolding procedure (shaded blue boxes). Where available, the results are compared to predictions made with the PYTHIA 8.309 event generator [86], with the majority of the uncertainties being too small to be visible.

Figures 6 and 7 display the normalized z distributions in $p_T(\text{jet})$ intervals for displaced and prompt $\psi(2S)$ meson production, respectively. Similarly, Figs. 8 and 9 provide the same distributions for the $\chi_{c1}(3872)$ meson production. The z distribution for each interval of $p_T(\text{jet})$ is normalized to unity.

A complementary set of results shows the fragmentation function differential in the $p_T(\text{tag})$ of the quarkonium. Figures 10 and 11 show the results for prompt and displaced $\psi(2S)$ meson production, respectively, and Figs. 12 and 13 show the results for prompt and displaced $\chi_{c1}(3872)$ meson production, respectively. In these complementary distributions, the z numerator, $p_T(\text{tag})$, effectively remains fixed while the denominator, $p_T(\text{jet})$, is no longer limited. This is in contrast to Figs. 6 to 9, where the numerator is not limited but the denominator is effectively fixed. This creates a subset of different probed kinematic regimes, as jets softer than the tag p_T window are not present in this representation.

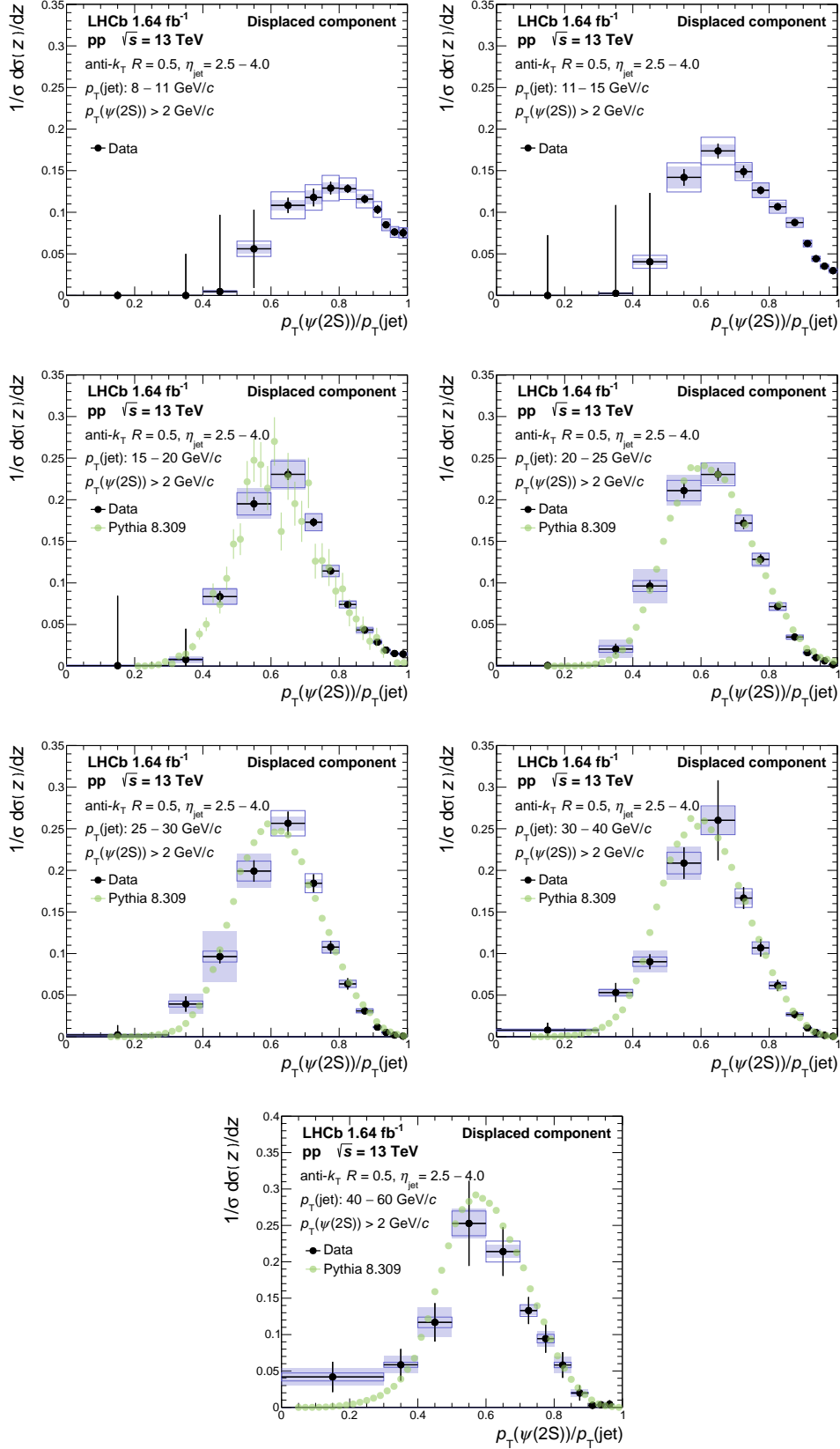


Figure 6: Distributions of the transverse momentum fraction z in intervals of jet p_T for displaced $\psi(2S)$ production with statistical (black error bars), correlated efficiency (empty blue boxes), and uncorrelated unfolding (shaded blue boxes) uncertainties, compared to predictions obtained from PYTHIA 8.309.

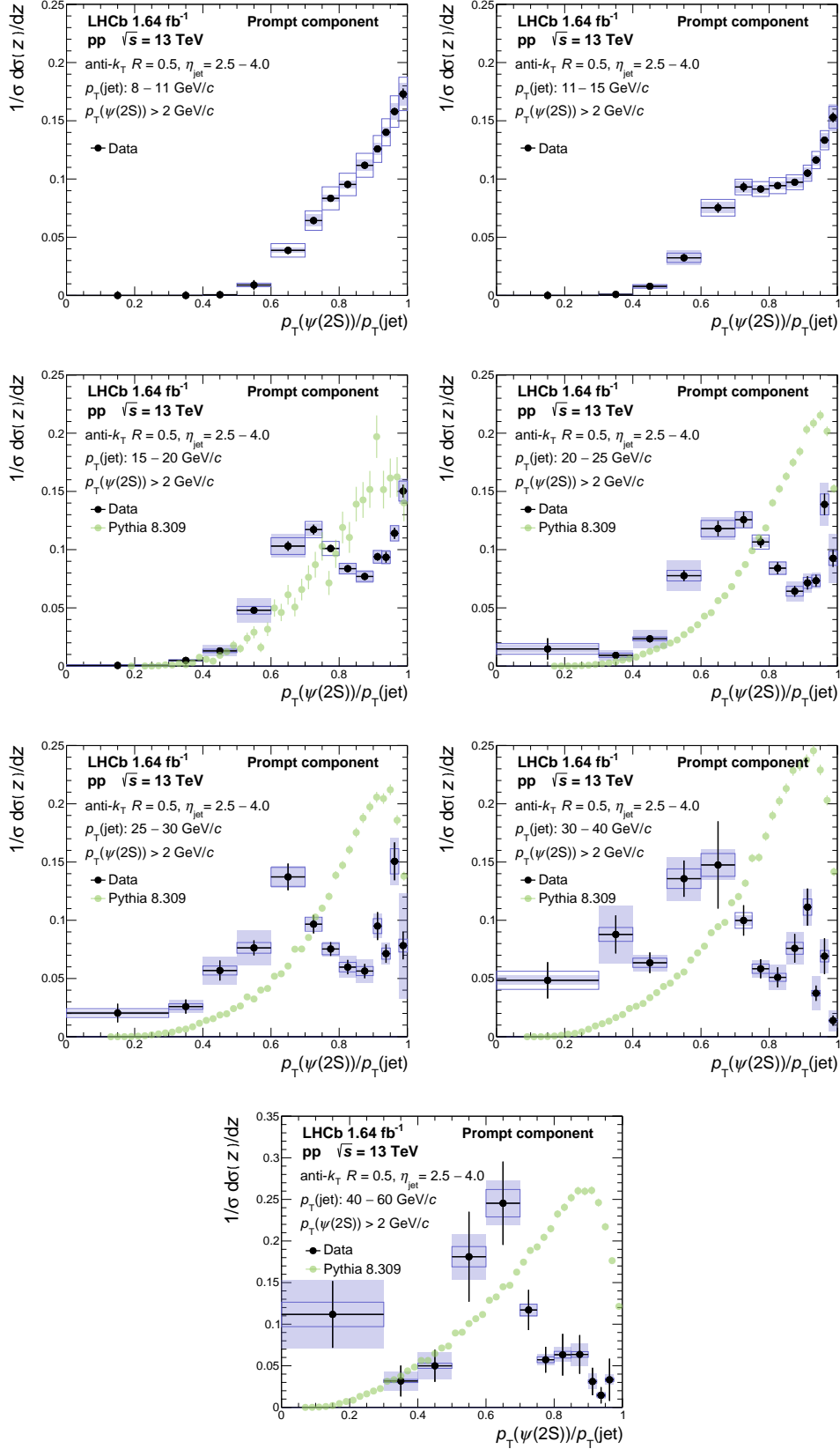


Figure 7: Distributions of the transverse momentum fraction z in intervals of jet p_T for prompt $\psi(2S)$ production with statistical (black error bars), correlated efficiency (empty blue boxes), and uncorrelated unfolding (shaded blue boxes) uncertainties, compared to predictions obtained from PYTHIA 8.309.

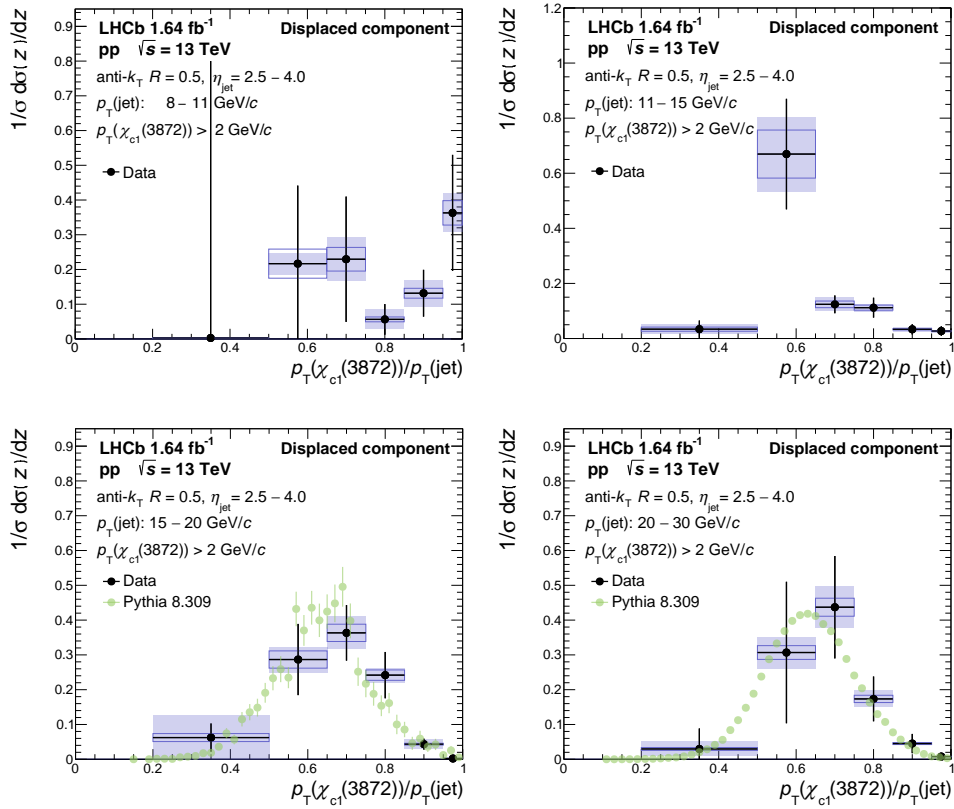


Figure 8: Distributions of the transverse momentum fraction z in intervals of jet p_T for displaced $\chi_{c1}(3872)$ production with statistical (black error bars), correlated efficiency (empty blue boxes), and uncorrelated unfolding (shaded blue boxes) uncertainties, compared to predictions obtained from PYTHIA 8.309.

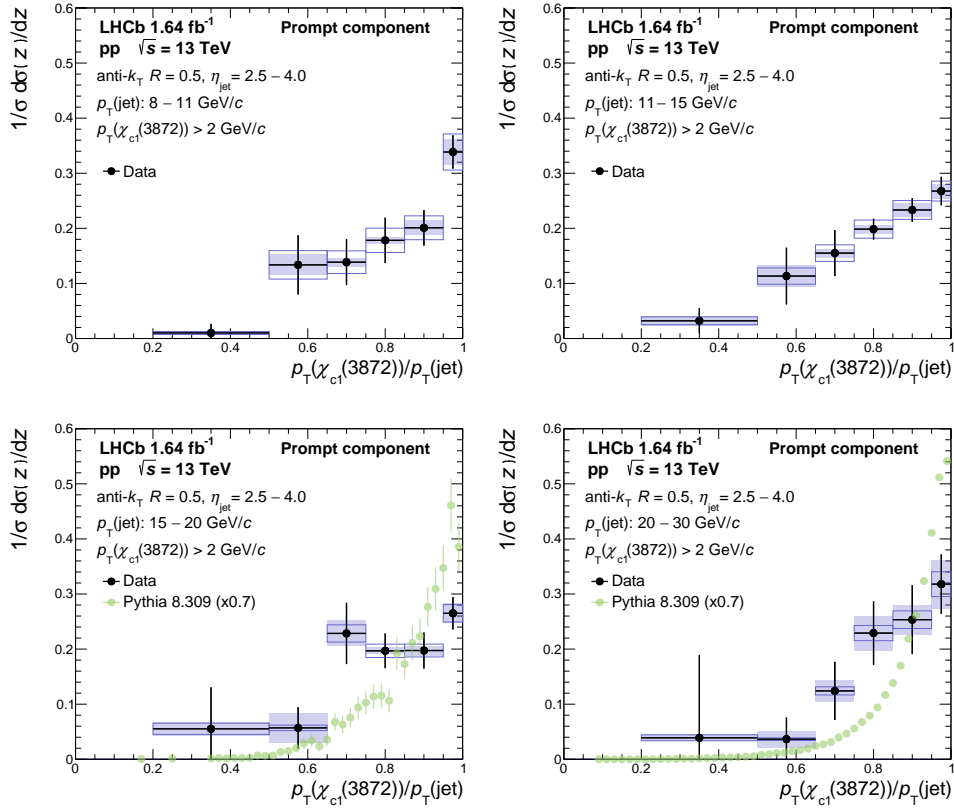


Figure 9: Distributions of the transverse momentum fraction z in intervals of jet p_T for prompt $\chi_{c1}(3872)$ production with statistical (black error bars), correlated efficiency (empty blue boxes), and uncorrelated unfolding (shaded blue boxes) uncertainties, compared to predictions obtained from PYTHIA 8.309.

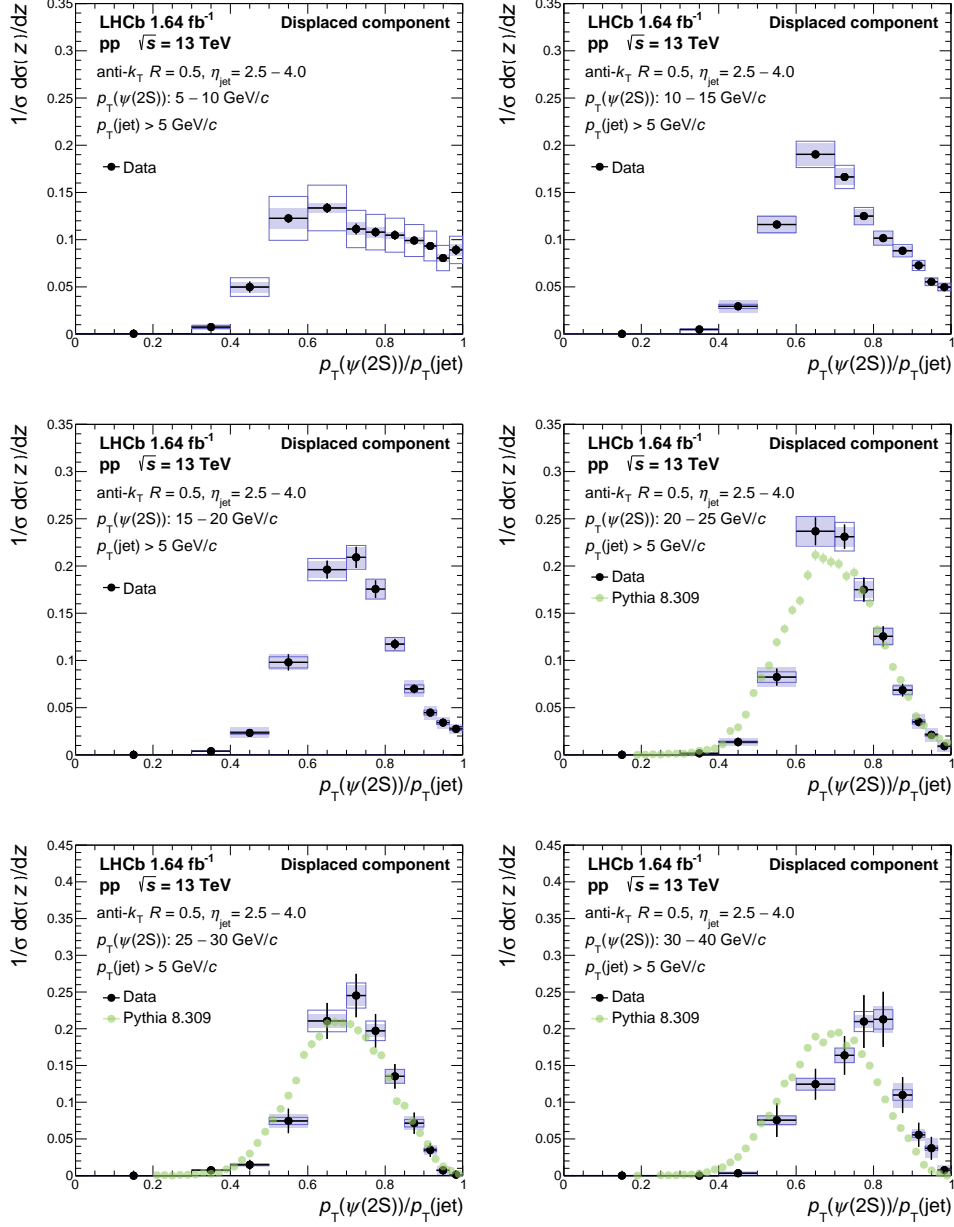


Figure 10: Distributions of the transverse momentum fraction z in intervals of $\psi(2S)$ p_T for displaced $\psi(2S)$ production with statistical (black error bars), correlated efficiency (empty blue boxes), and uncorrelated unfolding (shaded blue boxes) uncertainties, compared to predictions obtained from PYTHIA 8.309.

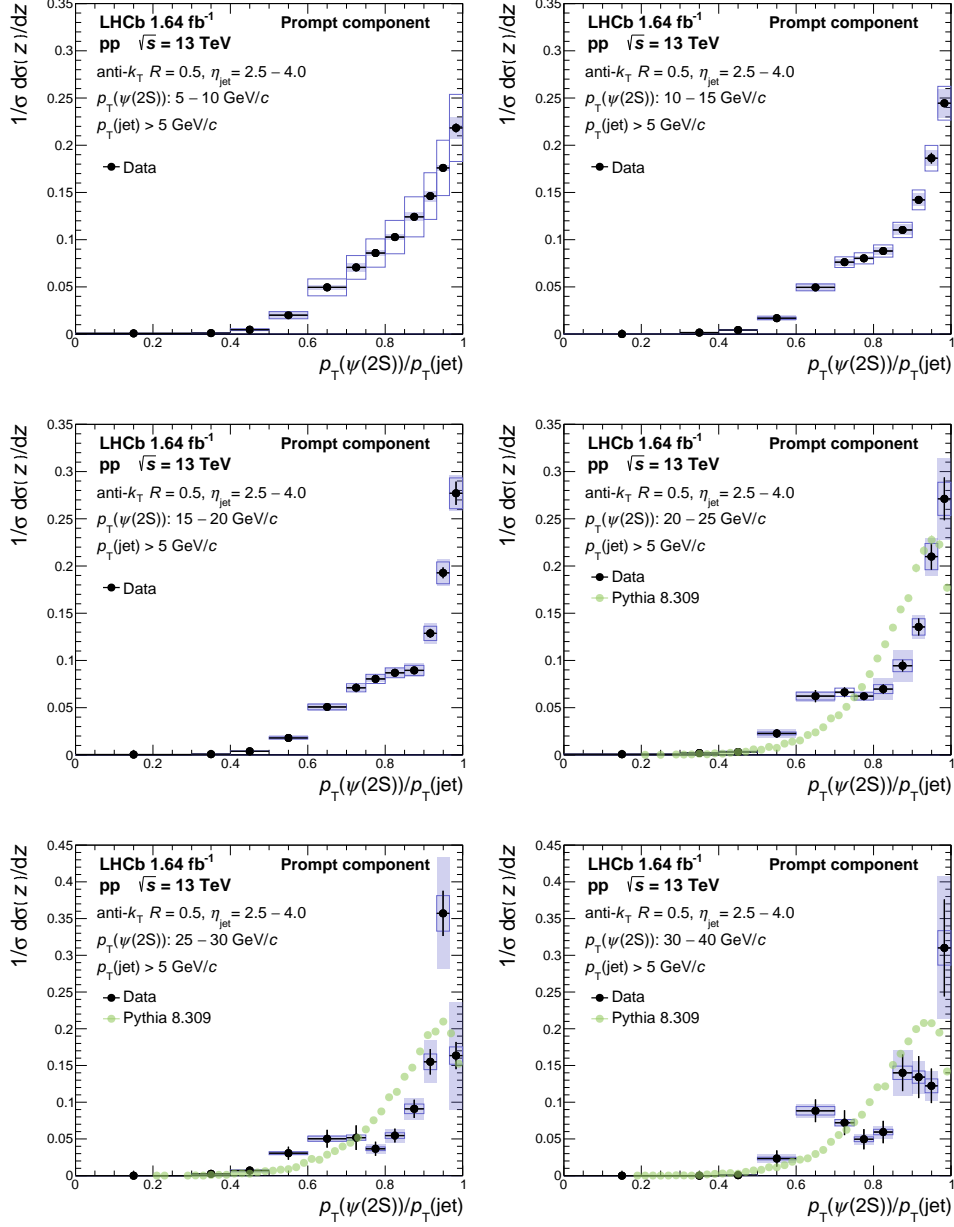


Figure 11: Distributions of the transverse momentum fraction z in intervals of $\psi(2S)$ p_T for prompt $\psi(2S)$ production with statistical (black error bars), correlated efficiency (empty blue boxes), and uncorrelated unfolding (shaded blue boxes) uncertainties, compared to predictions obtained from PYTHIA 8.309.

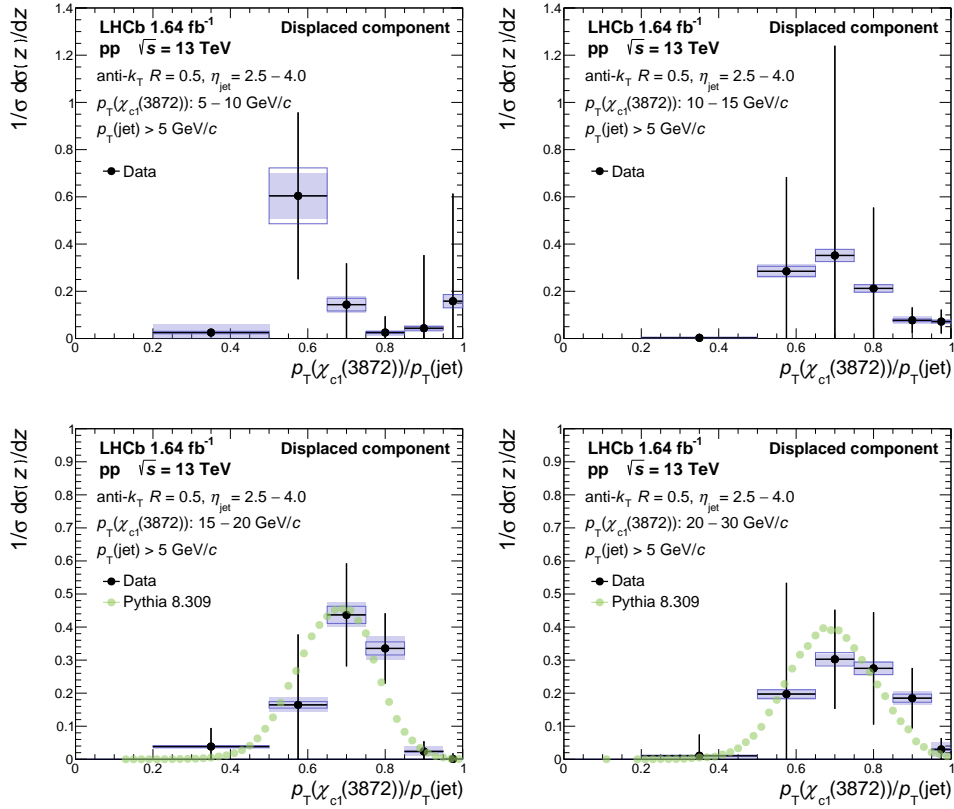


Figure 12: Distributions of the transverse momentum fraction z in intervals of $\chi_{c1}(3872) p_T$ for displaced $\chi_{c1}(3872)$ production with statistical (black error bars), correlated efficiency (empty blue boxes), and uncorrelated unfolding (shaded blue boxes) uncertainties, compared to predictions obtained from PYTHIA 8.309.

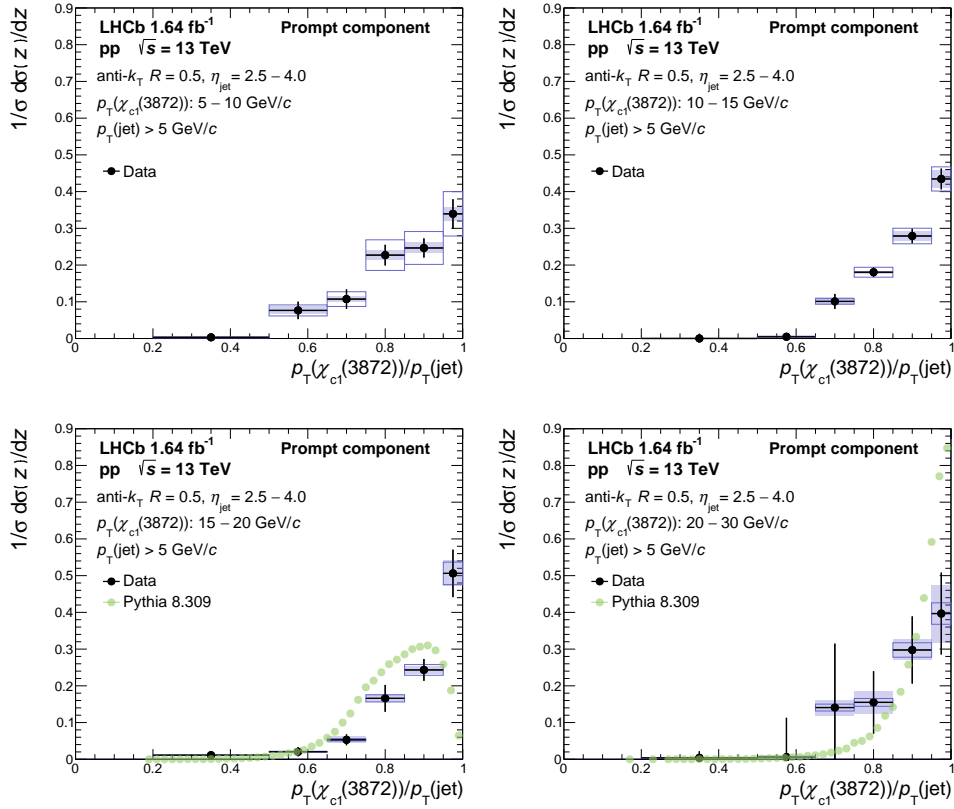


Figure 13: Distributions of the transverse momentum fraction z in intervals of $\chi_{c1}(3872)$ p_T for prompt $\chi_{c1}(3872)$ production with statistical (black error bars), correlated efficiency (empty blue boxes), and uncorrelated unfolding (shaded blue boxes) uncertainties, compared to predictions obtained from PYTHIA 8.309.

9 Conclusions

This paper reports the first study of $\psi(2S)$ and $\chi_{c1}(3872)$ production in jets. The analysis is based on proton-proton collision data collected by the LHCb experiment at the center-of-mass-energy of 13 TeV in 2016, corresponding to an integrated luminosity of 1.64 fb^{-1} . The differential distributions of the transverse momentum ratio between the quarkonium and the jet are measured with respect to both the jet and the quarkonium p_T . These distributions are further separated into prompt and displaced quarkonium production.

The z distributions from the displaced production of the $\psi(2S)$ and $\chi_{c1}(3872)$ mesons, as shown in Figs. 6, 8, 10 and 12, fall off rapidly as z approaches one. This production of quarkonia originates from the decay of b hadrons and is consequently accompanied by other decay products, which are typically clustered into the jet. The depleted yield below $z = 0.4$ is in part due to the fiducial limitations of this analysis. These distributions are well described by the PYTHIA 8.309 event generator, similarly to the results for displaced J/ψ meson production in jets [46, 48].

New insights can be gained from the z distributions for prompt production of $\psi(2S)$ and $\chi_{c1}(3872)$ mesons as they differ strikingly from predictions, as shown in Figs. 7, 9, 11 and 13. For distributions differential in both $p_T(\text{jet})$ and $p_T(\text{tag})$ two components appear to be visible. This is particularly evident in the $\psi(2S)$ meson case, which has a larger sample size and thus finer binning than the $\chi_{c1}(3872)$ results. The prompt $\psi(2S)$ distributions reveal a distinct component with $z \approx 1$ (isolated production) and another component centered around $z \approx 0.7$ (nonisolated production), which is more similar in shape to the displaced production in Fig. 6. The evolution of this pattern is best visible for the normalized z distributions in $p_T(\psi(2S))$ intervals. Here, the component of nonisolated $\psi(2S)$ yield is strongest at low $p_T(\psi(2S))$, while for the highest three $p_T(\psi(2S))$ intervals, the ratio of nonisolated yield and isolated yield appears to be roughly constant. Since the composition of different production mechanisms of quarkonia is dependent on the quarkonium p_T , the representation of the fragmentation function in $p_T(\text{jet})$ intervals is driven by the quarkonium p_T composition in each $p_T(\text{jet})$ interval, *e.g.* the highest $p_T(\text{jet})$ interval shows no yield at high z as the kinematic reach does not allow measuring $\psi(2S)$ mesons above $40 \text{ GeV}/c$ with sufficient abundance. The $\chi_{c1}(3872)$ results only hint at similar trends, but the sample sizes are too small to make any conclusive statements.

The exact nature of these two components in z for prompt $\psi(2S)$ and $\chi_{c1}(3872)$ production is not clear at this point. The data show, however, for the first time an isolated prompt production of quarkonia as expected from the NRQCD description of quarkonia production in the initial hard scattering. To explore the nature of the second component, which contains a significant fraction of prompt quarkonia production, further development of theoretical models is required.

Acknowledgements

We express our gratitude to our colleagues in the CERN accelerator departments for the excellent performance of the LHC. We thank the technical and administrative staff at the LHCb institutes. We acknowledge support from CERN and from the national agencies: CAPES, CNPq, FAPERJ and FINEP (Brazil); MOST and NSFC (China); CNRS/IN2P3 (France); BMBF, DFG and MPG (Germany); INFN (Italy); NWO (Netherlands); MNiSW

and NCN (Poland); MCID/IFA (Romania); MICIU and AEI (Spain); SNSF and SER (Switzerland); NASU (Ukraine); STFC (United Kingdom); DOE NP and NSF (USA). We acknowledge the computing resources that are provided by CERN, IN2P3 (France), KIT and DESY (Germany), INFN (Italy), SURF (Netherlands), PIC (Spain), GridPP (United Kingdom), CSCS (Switzerland), IFIN-HH (Romania), CBPF (Brazil), and Polish WLCG (Poland). We are indebted to the communities behind the multiple open-source software packages on which we depend. Individual groups or members have received support from ARC and ARDC (Australia); Key Research Program of Frontier Sciences of CAS, CAS PIFI, CAS CCEPP, Fundamental Research Funds for the Central Universities, and Sci. & Tech. Program of Guangzhou (China); Minciencias (Colombia); EPLANET, Marie Skłodowska-Curie Actions, ERC and NextGenerationEU (European Union); A*MIDEX, ANR, IPhU and Labex P2IO, and Région Auvergne-Rhône-Alpes (France); AvH Foundation (Germany); ICSC (Italy); Severo Ochoa and María de Maeztu Units of Excellence, GVA, XuntaGal, GENCAT, InTalent-Inditex and Prog. Atracción Talento CM (Spain); SRC (Sweden); the Leverhulme Trust, the Royal Society and UKRI (United Kingdom).

References

- [1] A. Martin, *Quarkonium*, Comments Nucl. Part. Phys. **16** (1986) 249.
- [2] A. G. Clark *et al.*, *Electron pair production at the CERN ISR*, Nucl. Phys. **B142** (1978) 29.
- [3] K. Ueno *et al.*, *Evidence for the Υ'' and a search for new narrow resonances*, Phys. Rev. Lett. **42** (1979) 486.
- [4] UA1 collaboration, C. Albajar *et al.*, *High transverse momentum J/ψ production at the CERN proton-antiproton collider*, Phys. Lett. **B200** (1988) 380.
- [5] UA1 collaboration, C. Albajar *et al.*, *Low mass dimuon production at the CERN proton-antiproton collider*, Phys. Lett. **B209** (1988) 397.
- [6] UA1 collaboration, C. Albajar *et al.*, *J/ψ and ψ' production at the CERN $p\bar{p}$ collider*, Phys. Lett. **B256** (1991) 112.
- [7] CDF collaboration, F. Abe *et al.*, *Production of J/ψ mesons from χ_c meson decays in $p\bar{p}$ collisions at $\sqrt{s} = 1.8$ TeV*, Phys. Rev. Lett. **79** (1997) 578.
- [8] CDF collaboration, D. Acosta *et al.*, *Measurement of the J/ψ meson and b-hadron production cross sections in $p\bar{p}$ collisions at $\sqrt{s} = 1960$ GeV*, Phys. Rev. **D71** (2005) 032001, arXiv:hep-ex/0412071.
- [9] D0 collaboration, S. Abachi *et al.*, *J/ψ production in $p\bar{p}$ collisions at $\sqrt{s} = 1.8$ TeV*, Phys. Lett. **B370** (1996) 239.
- [10] PHENIX collaboration, A. Adare *et al.*, *Ground and excited charmonium state production in $p + p$ collisions at $\sqrt{s} = 200$ GeV*, Phys. Rev. **D85** (2012) 092004, arXiv:1105.1966.
- [11] LHCb collaboration, R. Aaij *et al.*, *Measurement of forward J/ψ production cross-sections in pp collisions at $\sqrt{s} = 13$ TeV*, JHEP **10** (2015) 172, Erratum ibid. **05** (2017) 063, arXiv:1509.00771.
- [12] LHCb collaboration, R. Aaij *et al.*, *Production of J/ψ and Υ mesons in pp collisions at $\sqrt{s} = 8$ TeV*, JHEP **06** (2013) 064, arXiv:1304.6977.
- [13] LHCb collaboration, R. Aaij *et al.*, *Measurement of J/ψ production in pp collisions at $\sqrt{s} = 2.76$ TeV*, JHEP **02** (2013) 041, arXiv:1212.1045.
- [14] LHCb collaboration, R. Aaij *et al.*, *Measurement of J/ψ production in pp collisions at $\sqrt{s} = 7$ TeV*, Eur. Phys. J. **C71** (2011) 1645, arXiv:1103.0423.
- [15] ATLAS collaboration, G. Aad *et al.*, *Measurement of the differential cross-sections of prompt and non-prompt production of J/ψ and $\psi(2S)$ in pp collisions at $\sqrt{s} = 7$ and 8 TeV with the ATLAS detector*, Eur. Phys. J. **C76** (2016) 283, arXiv:1512.03657.
- [16] CMS collaboration, V. Khachatryan *et al.*, *Measurement of J/ψ and $\psi(2S)$ prompt double-differential cross sections in pp collisions at $\sqrt{s} = 7$ TeV*, Phys. Rev. Lett. **114** (2015) 191802, arXiv:1502.04155.

- [17] ALICE collaboration, B. Abelev *et al.*, *Inclusive J/ψ production in pp collisions at $\sqrt{s} = 2.76$ TeV*, Phys. Lett. **B718** (2012) 295, Erratum *ibid.* **B748** (2015) 472, [arXiv:1203.3641](#).
- [18] LHCb collaboration, R. Aaij *et al.*, *Measurement of the cross-section ratio $\sigma(\chi_{c2})/\sigma(\chi_{c1})$ for prompt χ_c production at $\sqrt{s} = 7$ TeV*, Phys. Lett. **B714** (2012) 215, [arXiv:1202.1080](#).
- [19] LHCb collaboration, R. Aaij *et al.*, *Measurement of $\psi(2S)$ production cross-sections in proton-proton collisions at $\sqrt{s} = 7$ and 13 TeV*, Eur. Phys. J. **C80** (2020) 185, [arXiv:1908.03099](#).
- [20] LHCb collaboration, R. Aaij *et al.*, *Measurement of Υ production cross-section in pp collisions at $\sqrt{s} = 13$ TeV*, JHEP **07** (2018) 134, [arXiv:1804.09214](#).
- [21] CMS collaboration, A. M. Sirunyan *et al.*, *Measurement of quarkonium production cross sections in pp collisions at $\sqrt{s} = 13$ TeV*, Phys. Lett. **B780** (2018) 251, [arXiv:1710.11002](#).
- [22] ATLAS collaboration, G. Aad *et al.*, *Measurement of the production cross-section of J/ψ and $\psi(2S)$ mesons in pp collisions at $\sqrt{s} = 13$ TeV with the ATLAS detector*, Eur. Phys. J. **C84** (2024) 169, [arXiv:2309.17177](#).
- [23] G. T. Bodwin, E. Braaten, and G. P. Lepage, *Rigorous QCD analysis of inclusive annihilation and production of heavy quarkonium*, Phys. Rev. **D51** (1995) 1125, Erratum *ibid.* **D55** (1997) 5853, [arXiv:hep-ph/9407339](#).
- [24] P. L. Cho and A. K. Leibovich, *Color octet quarkonia production*, Phys. Rev. **D53** (1996) 150, [arXiv:hep-ph/9505329](#).
- [25] P. L. Cho and A. K. Leibovich, *Color octet quarkonia production. 2.*, Phys. Rev. **D53** (1996) 6203, [arXiv:hep-ph/9511315](#).
- [26] J. M. Campbell, F. Maltoni, and F. Tramontano, *QCD corrections to J/ψ and Υ production at hadron colliders*, Phys. Rev. Lett. **98** (2007) 252002, [arXiv:hep-ph/0703113](#).
- [27] J. P. Lansberg, *On the mechanisms of heavy-quarkonium hadroproduction*, Eur. Phys. J. **C61** (2009) 693, [arXiv:0811.4005](#).
- [28] B. Gong and J.-X. Wang, *Next-to-leading-order QCD corrections to J/ψ polarization at Tevatron and Large-Hadron-Collider energies*, Phys. Rev. Lett. **100** (2008) 232001, [arXiv:0802.3727](#).
- [29] A. K. Leibovich, *ψ' polarization due to color octet quarkonia production*, Phys. Rev. **D56** (1997) 4412, [arXiv:hep-ph/9610381](#).
- [30] E. Braaten and J. Lee, *Polarization of v_{nS} at the Tevatron*, Phys. Rev. **D63** (2001) 071501, [arXiv:hep-ph/0012244](#).
- [31] M. Beneke and M. Krämer, *Direct J/ψ and ψ' polarization and cross-sections at the Tevatron*, Phys. Rev. **D55** (1997) 5269, [arXiv:hep-ph/9611218](#).

- [32] E. Braaten, B. A. Kniehl, and J. Lee, *Polarization of prompt J/ψ at the Tevatron*, Phys. Rev. **D62** (2000) 094005, arXiv:hep-ph/9911436.
- [33] B. Gong, L.-P. Wan, J.-X. Wang, and H.-F. Zhang, *Polarization for Prompt J/ψ and $\psi(2s)$ production at the Tevatron and LHC*, Phys. Rev. Lett. **110** (2013) 042002, arXiv:1205.6682.
- [34] K.-T. Chao *et al.*, *J/ψ polarization at hadron colliders in nonrelativistic QCD*, Phys. Rev. Lett. **108** (2012) 242004, arXiv:1201.2675.
- [35] LHCb collaboration, R. Aaij *et al.*, *Measurement of J/ψ polarization in pp collisions at $\sqrt{s} = 7$ TeV*, Eur. Phys. J. **C73** (2013) 2631, arXiv:1307.6379.
- [36] LHCb collaboration, R. Aaij *et al.*, *Measurement of $\psi(2S)$ polarisation in pp collisions at $\sqrt{s} = 7$ TeV*, Eur. Phys. J. **C74** (2014) 2872, arXiv:1403.1339.
- [37] ALICE collaboration, B. Abelev *et al.*, *J/ψ polarization in pp collisions at $\sqrt{s} = 7$ TeV*, Phys. Rev. Lett. **108** (2012) 082001, arXiv:1111.1630.
- [38] CDF collaboration, A. Abulencia *et al.*, *Polarization of J/ψ and $\psi(2S)$ mesons produced in $p\bar{p}$ collisions at $\sqrt{s} = 1.96$ TeV*, Phys. Rev. Lett. **99** (2007) 132001, arXiv:0704.0638.
- [39] CMS collaboration, S. Chatrchyan *et al.*, *Measurement of the prompt J/ψ and $\psi(2S)$ polarizations in pp collisions at $\sqrt{s} = 7$ TeV*, Phys. Lett. **B727** (2013) 381, arXiv:1307.6070.
- [40] ALICE collaboration, S. Acharya *et al.*, *Measurement of the inclusive J/ψ polarization at forward rapidity in pp collisions at $\sqrt{s} = 8$ TeV*, Eur. Phys. J. **C78** (2018) 562, arXiv:1805.04374.
- [41] ALICE collaboration, S. Acharya *et al.*, *First measurement of quarkonium polarization in nuclear collisions at the LHC*, Phys. Lett. **B815** (2021) 136146, arXiv:2005.11128.
- [42] STAR collaboration, J. Adam *et al.*, *Measurement of inclusive J/ψ polarization in $p + p$ collisions at $\sqrt{s} = 200$ GeV by the STAR experiment*, Phys. Rev. **D102** (2020) 092009, arXiv:2007.04732.
- [43] PHENIX collaboration, U. Acharya *et al.*, *Polarization and cross section of midrapidity J/ψ production in $p + p$ collisions at $\sqrt{s} = 510$ GeV*, Phys. Rev. **D102** (2020) 072008, arXiv:2005.14273.
- [44] J.-P. Lansberg, *New observables in inclusive production of quarkonia*, Phys. Rept. **889** (2020) 1, arXiv:1903.09185.
- [45] H. S. Chung, *Review of quarkonium production: status and prospects*, PoS **Confinement2018** (2018) 007, arXiv:1811.12098.
- [46] LHCb collaboration, R. Aaij *et al.*, *Study of J/ψ production in jets*, Phys. Rev. Lett. **118** (2017) 192001, arXiv:1701.05116.

- [47] CMS collaboration, A. M. Sirunyan *et al.*, *Study of J/ψ meson production inside jets in pp collisions at $\sqrt{s} = 8$ TeV*, Phys. Lett. **B804** (2020) 135409, arXiv:1910.01686.
- [48] CMS collaboration, A. Tumasyan *et al.*, *Fragmentation of jets containing a prompt J/ψ meson in $PbPb$ and pp collisions at $\sqrt{s_{NN}} = 5.02$ TeV*, Phys. Lett. **B825** (2022) 136842, arXiv:2106.13235.
- [49] R. Bain, Y. Makris, and T. Mehen, *Transverse momentum dependent fragmenting jet functions with applications to quarkonium production*, JHEP **11** (2016) 144, arXiv:1610.06508.
- [50] R. Bain *et al.*, *NRQCD confronts LHCb data on quarkonium production within jets*, Phys. Rev. Lett. **119** (2017) 032002, arXiv:1702.05525.
- [51] N. Cooke, P. Ilten, L. Lönnblad, and S. Mrenna, *Non-relativistic quantum chromodynamics in parton showers*, Eur. Phys. J. **C84** (2024) 432, arXiv:2312.05203.
- [52] T. Matsui and H. Satz, *J/ψ suppression by quark-gluon plasma formation*, Phys. Lett. **B178** (1986) 416.
- [53] ALICE collaboration, S. Acharya *et al.*, *Measurement of the production of charm jets tagged with D^0 mesons in pp collisions at $\sqrt{s} = 5.02$ and 13 TeV*, JHEP **06** (2023) 133, arXiv:2204.10167.
- [54] ALICE collaboration, S. Acharya *et al.*, *Measurement of the production of charm jets tagged with D^0 mesons in pp collisions at $\sqrt{s} = 7$ TeV*, JHEP **08** (2019) 133, arXiv:1905.02510.
- [55] UA1 collaboration, C. Albajar *et al.*, *A study of the D^* content of jets at the CERN $p\bar{p}$ collider*, Phys. Lett. **B244** (1990) 566.
- [56] STAR Collaboration, B. I. Abelev *et al.*, *Measurement of D^* mesons in jets from $p + p$ collisions at $\sqrt{s} = 200$ GeV*, Phys. Rev. **D79** (2009) 112006.
- [57] ATLAS collaboration, G. Aad *et al.*, *Measurement of $D^{*\pm}$ meson production in jets from pp collisions at $\sqrt{s} = 7$ TeV with the ATLAS detector*, Phys. Rev. **D85** (2012) 052005, arXiv:1112.4432.
- [58] H1 collaboration, F. D. Aaron *et al.*, *Measurement of inclusive and dijet D^* meson cross sections in photoproduction at HERA*, Eur. Phys. J. **C72** (2012) 1995, arXiv:1203.1170.
- [59] ZEUS collaboration, S. Chekanov *et al.*, *Measurement of the charm fragmentation function in D^* photoproduction at HERA*, JHEP **04** (2009) 082, arXiv:0901.1210.
- [60] ATLAS collaboration, G. Aad *et al.*, *Measurement of b -quark fragmentation properties in jets using the decay $B^\pm \rightarrow J/\psi K^\pm$ in pp collisions at $\sqrt{s} = 13$ TeV with the ATLAS detector*, JHEP **12** (2021) 131, arXiv:2108.11650.
- [61] ALICE collaboration, S. Acharya *et al.*, *Measurement of the fraction of jet longitudinal momentum carried by Λ_c^+ baryons in pp collisions*, Phys. Rev. **D109** (2024) 072005, arXiv:2301.13798.

- [62] LHCb collaboration, R. Aaij *et al.*, *Measurement of $\psi(2S)$ meson production in pp collisions at $\sqrt{s} = 7$ TeV*, Eur. Phys. J. **C72** (2012) 2100, Erratum *ibid.* **C80** (2020) 49, [arXiv:1204.1258](#).
- [63] LHCb collaboration, A. A. Alves Jr. *et al.*, *The LHCb detector at the LHC*, JINST **3** (2008) S08005.
- [64] LHCb collaboration, R. Aaij *et al.*, *LHCb detector performance*, Int. J. Mod. Phys. **A30** (2015) 1530022, [arXiv:1412.6352](#).
- [65] A. A. Alves Jr. *et al.*, *Performance of the LHCb muon system*, JINST **8** (2013) P02022, [arXiv:1211.1346](#).
- [66] R. Aaij *et al.*, *The LHCb trigger and its performance in 2011*, JINST **8** (2013) P04022, [arXiv:1211.3055](#).
- [67] Particle Data Group, S. Navas *et al.*, *Review of particle physics*, Phys. Rev. **D110** (2024) 030001.
- [68] R. Aaij *et al.*, *Tesla: An application for real-time data analysis in High Energy Physics*, Comput. Phys. Commun. **208** (2016) 35, [arXiv:1604.05596](#).
- [69] G. Dujany and B. Storaci, *Real-time alignment and calibration of the LHCb Detector in Run II*, J. Phys. Conf. Ser. **664** (2015) 082010.
- [70] T. Sjöstrand, S. Mrenna, and P. Skands, *A brief introduction to PYTHIA 8.1*, Comput. Phys. Commun. **178** (2008) 852, [arXiv:0710.3820](#).
- [71] I. Belyaev *et al.*, *Handling of the generation of primary events in Gauss, the LHCb simulation framework*, J. Phys. Conf. Ser. **331** (2011) 032047.
- [72] D. J. Lange, *The EvtGen particle decay simulation package*, Nucl. Instrum. Meth. **A462** (2001) 152.
- [73] N. Davidson, T. Przedzinski, and Z. Was, *PHOTOS interface in C++: Technical and physics documentation*, Comp. Phys. Comm. **199** (2016) 86, [arXiv:1011.0937](#).
- [74] Geant4 collaboration, J. Allison *et al.*, *Geant4 developments and applications*, IEEE Trans. Nucl. Sci. **53** (2006) 270; Geant4 collaboration, S. Agostinelli *et al.*, *Geant4: A simulation toolkit*, Nucl. Instrum. Meth. **A506** (2003) 250.
- [75] M. Clemencic *et al.*, *The LHCb simulation application, Gauss: Design, evolution and experience*, J. Phys. Conf. Ser. **331** (2011) 032023.
- [76] LHCb collaboration, R. Aaij *et al.*, *Observation of sizeable ω contribution to $\chi_{c1} \rightarrow \pi^+\pi^-J/\psi$ decays*, [arXiv:2204.12597](#), to appear in Phys. Rev. D.
- [77] LHCb collaboration, R. Aaij *et al.*, *Study of forward Z +jet production in pp collisions at $\sqrt{s} = 7$ TeV*, JHEP **01** (2014) 033, [arXiv:1310.8197](#).
- [78] M. Cacciari, G. P. Salam, and G. Soyez, *The anti- k_t jet clustering algorithm*, JHEP **04** (2008) 063, [arXiv:0802.1189](#).

- [79] M. Cacciari, G. P. Salam, and G. Soyez, *FastJet user manual*, Eur. Phys. J. **C72** (2012) 1896, [arXiv:1111.6097](#).
- [80] T. Skwarnicki, *A study of the radiative cascade transitions between the Upsilon-prime and Upsilon resonances*, PhD thesis, Institute of Nuclear Physics, Krakow, 1986, DESY-F31-86-02.
- [81] LHCb collaboration, R. Aaij *et al.*, *Measurement of $\chi_{c1}(3872)$ production in proton-proton collisions at $\sqrt{s} = 8$ and 13 TeV*, JHEP **01** (2022) 131, [arXiv:2109.07360](#).
- [82] LHCb collaboration, R. Aaij *et al.*, *Measurement of the track reconstruction efficiency at LHCb*, JINST **10** (2015) P02007, [arXiv:1408.1251](#).
- [83] S. Tolk, J. Albrecht, F. Dettori, and A. Pellegrino, *Data driven trigger efficiency determination at LHCb*, LHCb-PUB-2014-039, 2014.
- [84] G. D’Agostini, *A multidimensional unfolding method based on Bayes’ theorem*, Nucl. Instrum. Meth. **A362** (1995) 487.
- [85] T. Adye, *Unfolding algorithms and tests using RooUnfold*, in *PHYSTAT 2011*, (Geneva), 313–318, CERN, 2011, [arXiv:1105.1160](#).
- [86] C. Bierlich *et al.*, *A comprehensive guide to the physics and usage of PYTHIA 8.3*, SciPost Phys. Codeb. **2022** (2022) 8, [arXiv:2203.11601](#).

LHCb collaboration

R. Aaij³⁶, A.S.W. Abdelmotteleb⁵⁵, C. Abellan Beteta⁴⁹, F. Abudinén⁵⁵,
T. Ackernley⁵⁹, A. A. Adefisoye⁶⁷, B. Adeva⁴⁵, M. Adinolfi⁵³, P. Adlarson⁸⁰,
C. Agapopoulou¹³, C.A. Aidala⁸¹, Z. Ajaltouni¹¹, S. Akar⁶⁴, K. Akiba³⁶,
P. Albicocco²⁶, J. Albrecht^{18,g}, F. Alessio⁴⁷, M. Alexander⁵⁸, Z. Aliouche⁶¹,
P. Alvarez Cartelle⁵⁴, R. Amalric¹⁵, S. Amato³, J.L. Amey⁵³, Y. Amhis^{13,47},
L. An⁶, L. Anderlini²⁵, M. Andersson⁴⁹, A. Andreianov⁴², P. Andreola⁴⁹,
M. Andreotti²⁴, D. Andreou⁶⁷, A. Anelli^{29,p}, D. Ao⁷, F. Archilli^{35,v},
M. Argenton²⁴, S. Arguedas Cuendis^{9,47}, A. Artamonov⁴², M. Artuso⁶⁷,
E. Aslanides¹², R. Ataíde Da Silva⁴⁸, M. Atzeni⁶³, B. Audurier¹⁴, D. Bacher⁶²,
I. Bachiller Perea¹⁰, S. Bachmann²⁰, M. Bachmayer⁴⁸, J.J. Back⁵⁵,
P. Baladron Rodriguez⁴⁵, V. Balagura¹⁴, W. Baldini²⁴, L. Balzani¹⁸, H. Bao⁷,
J. Baptista de Souza Leite⁵⁹, C. Barbero Pretel^{45,82}, M. Barbetti²⁵, I. R. Barbosa⁶⁸,
R.J. Barlow⁶¹, M. Barnyakov²³, S. Barsuk¹³, W. Barter⁵⁷, M. Bartolini⁵⁴,
J. Bartz⁶⁷, J.M. Basels¹⁶, S. Bashir³⁸, G. Bassi^{33,s}, B. Batsukh⁵, P. B. Battista¹³,
A. Bay⁴⁸, A. Beck⁵⁵, M. Becker¹⁸, F. Bedeschi³³, I.B. Bediaga², N. A.
Behling¹⁸, S. Belin⁴⁵, V. Bellee⁴⁹, K. Belous⁴², I. Belov²⁷, I. Belyaev³⁴,
G. Benane¹², G. Bencivenni²⁶, E. Ben-Haim¹⁵, A. Berezhnoy⁴², R. Bernet⁴⁹,
S. Bernet Andres⁴³, A. Bertolin³¹, C. Betancourt⁴⁹, F. Betti⁵⁷, J. Bex⁵⁴,
Ia. Bezshyiko⁴⁹, J. Bhom³⁹, M.S. Bieker¹⁸, N.V. Biesuz²⁴, P. Billoir¹⁵,
A. Biolchini³⁶, M. Birch⁶⁰, F.C.R. Bishop¹⁰, A. Bitadze⁶¹, A. Bizzeti¹⁵, T. Blake⁵⁵,
F. Blanc⁴⁸, J.E. Blank¹⁸, S. Blusk⁶⁷, V. Bocharnikov⁴², J.A. Boelhave¹⁸,
O. Boente Garcia¹⁴, T. Boettcher⁶⁴, A. Bohare⁵⁷, A. Boldyrev⁴², C.S. Bolognani⁷⁷,
R. Bolzonella^{24,m}, N. Bondar⁴², A. Bordelius⁴⁷, F. Borgato^{31,q}, S. Borghi⁶¹,
M. Borsato^{29,p}, J.T. Borsuk³⁹, S.A. Bouchiba⁴⁸, M. Bovill⁶², T.J.V. Bowcock⁵⁹,
A. Boyer⁴⁷, C. Bozzi²⁴, A. Brea Rodriguez⁴⁸, N. Breer¹⁸, J. Brodzicka³⁹,
A. Brossa Gonzalo^{45,55,44,†}, J. Brown⁵⁹, D. Brundu³⁰, E. Buchanan⁵⁷, A. Buonauro⁴⁹,
L. Buonincontri^{31,q}, A.T. Burke⁶¹, C. Burr⁴⁷, J.S. Butter⁵⁴, J. Buytaert⁴⁷,
W. Byczynski⁴⁷, S. Cadeddu³⁰, H. Cai⁷², A. C. Caillet¹⁵, R. Calabrese^{24,m},
S. Calderon Ramirez⁹, L. Calefice⁴⁴, S. Cali²⁶, M. Calvi^{29,p}, M. Calvo Gomez⁴³,
P. Camargo Magalhaes^{2,z}, J. I. Cambon Bouzas⁴⁵, P. Campana²⁶,
D.H. Campora Perez⁷⁷, A.F. Campoverde Quezada⁷, S. Capelli²⁹, L. Capriotti²⁴,
R. Caravaca-Mora⁹, A. Carbone^{23,k}, L. Carcedo Salgado⁴⁵, R. Cardinale^{27,n},
A. Cardini³⁰, P. Carniti^{29,p}, L. Carus²⁰, A. Casais Vidal⁶³, R. Caspary²⁰,
G. Casse⁵⁹, J. Castro Godinez⁹, M. Cattaneo⁴⁷, G. Cavallero^{24,47}, V. Cavallini^{24,m},
S. Celani²⁰, D. Cervenkov⁶², S. Cesare^{28,o}, A.J. Chadwick⁵⁹, I. Chahrour⁸¹,
M. Charles¹⁵, Ph. Charpentier⁴⁷, E. Chatzianagnostou³⁶, M. Chefdeville¹⁰,
C. Chen¹², S. Chen⁵, Z. Chen⁷, A. Chernov³⁹, S. Chernyshenko⁵¹, X.
Chiotopoulos⁷⁷, V. Chobanova⁷⁹, S. Cholak⁴⁸, M. Chruszcz³⁹, A. Chubykin⁴²,
V. Chulikov⁴², P. Ciambone²⁶, X. Cid Vidal⁴⁵, G. Ciezarek⁴⁷, P. Cifra⁴⁷,
P.E.L. Clarke⁵⁷, M. Clemencic⁴⁷, H.V. Cliff⁵⁴, J. Closier⁴⁷, C. Cocha Toapaxi²⁰,
V. Coco⁴⁷, J. Cogan¹², E. Cogneras¹¹, L. Cojocariu⁴¹, P. Collins⁴⁷,
T. Colombo⁴⁷, M. C. Colonna¹⁸, A. Comerma-Montells⁴⁴, L. Congedo²²,
A. Contu³⁰, N. Cooke⁵⁸, I. Corredoira⁴⁵, A. Correia¹⁵, G. Corti⁴⁷,
J.J. Cottee Meldrum⁵³, B. Couturier⁴⁷, D.C. Craik⁴⁹, M. Cruz Torres^{2,h},
E. Curras Rivera⁴⁸, R. Currie⁵⁷, C.L. Da Silva⁶⁶, S. Dadabaev⁴², L. Dai⁶⁹,
X. Dai⁶, E. Dall’Occo¹⁸, J. Dalseno⁴⁵, C. D’Ambrosio⁴⁷, J. Daniel¹¹,
A. Danilina⁴², P. d’Argent²², A. Davidson⁵⁵, J.E. Davies⁶¹, A. Davis⁶¹,
O. De Aguiar Francisco⁶¹, C. De Angelis^{30,l}, F. De Benedetti⁴⁷, J. de Boer³⁶,

S. Kandybei⁵⁰, M. Kane⁵⁷, Y. Kang^{4,c}, C. Kar¹¹, M. Karacson⁴⁷,
D. Karpenkov⁴², A. Kauniskangas⁴⁸, J.W. Kautz⁶⁴, M.K. Kazanecki³⁹, F. Keizer⁴⁷,
M. Kenzie⁵⁴, T. Ketel³⁶, B. Khanji⁶⁷, A. Kharisova⁴², S. Kholodenko^{33,47},
G. Khreich¹³, T. Kirn¹⁶, V.S. Kirsebom^{29,p}, O. Kitouni⁶³, S. Klaver³⁷,
N. Kleijne^{33,s}, K. Klimaszewski⁴⁰, M.R. Kmiec⁴⁰, S. Koliiev⁵¹, L. Kolk¹⁸,
A. Konoplyannikov⁴², P. Kopciwicz^{38,47}, P. Koppenburg³⁶, M. Koroley⁴²,
I. Kostyuk³⁶, O. Kot⁵¹, S. Kotriakhova, A. Kozachuk⁴², P. Kravchenko⁴²,
L. Kravchuk⁴², M. Kreps⁵⁵, P. Krokovny⁴², W. Krupa⁶⁷, W. Krzemien⁴⁰,
O. Kshyvanskyi⁵¹, J. Kubat²⁰, S. Kubis⁷⁸, M. Kucharczyk³⁹, V. Kudryavtsev⁴²,
E. Kulikova⁴², A. Kupsc⁸⁰, B.K. Kutsenko¹², D. Lacarrere⁴⁷, P.
Laguarta Gonzalez⁴⁴, A. Lai³⁰, A. Lampis³⁰, D. Lancierini⁵⁴, C. Landesa Gomez⁴⁵,
J.J. Lane¹, R. Lane⁵³, G. Lanfranchi²⁶, C. Langenbruch²⁰, J. Langer¹⁸,
O. Lantwin⁴², T. Latham⁵⁵, F. Lazzari^{33,t}, C. Lazzeroni⁵², R. Le Gac¹², H.
Lee⁵⁹, R. Lefèvre¹¹, A. Leflat⁴², S. Legotin⁴², M. Lehuraux⁵⁵, E. Lemos Cid⁴⁷,
O. Leroy¹², T. Lesiak³⁹, E. D. Lesser⁴⁷, B. Leverington²⁰, A. Li^{4,c}, C. Li¹²,
H. Li⁷⁰, K. Li⁸, L. Li⁶¹, P. Li⁷, P.-R. Li⁷¹, Q. Li^{5,7}, S. Li⁸, T. Li^{5,e},
T. Li⁷⁰, Y. Li⁸, Y. Li⁵, Z. Lian^{4,c}, X. Liang⁶⁷, S. Libralon⁴⁶, C. Lin⁷, T. Lin⁵⁶,
R. Lindner⁴⁷, V. Lisovskyi⁴⁸, R. Litvinov^{30,47}, F. L. Liu¹, G. Liu⁷⁰, K. Liu⁷¹,
S. Liu^{5,7}, W. Liu⁸, Y. Liu⁵⁷, Y. Liu⁷¹, Y. L. Liu⁶⁰, A. Lobo Salvia⁴⁴, A. Loi³⁰,
J. Lomba Castro⁴⁵, T. Long⁵⁴, J.H. Lopes³, A. Lopez Huertas⁴⁴, S. López Soliño⁴⁵,
Q. Lu¹⁴, C. Lucarelli²⁵, D. Lucchesi^{31,q}, M. Lucio Martinez⁷⁷, V. Lukashenko^{36,51},
Y. Luo⁶, A. Lupato^{31,j}, E. Luppi^{24,m}, K. Lynch²¹, X.-R. Lyu⁷, G. M. Ma^{4,c},
R. Ma⁷, S. Maccolini¹⁸, F. Machefert¹³, F. Maciuc⁴¹, B. Mack⁶⁷, I. Mackay⁶², L.
M. Mackey⁶⁷, L.R. Madhan Mohan⁵⁴, M. J. Madurai⁵², A. Maevskiy⁴²,
D. Magdalinski³⁶, D. Maisuzenko⁴², M.W. Majewski³⁸, J.J. Malczewski³⁹, S. Malde⁶²,
L. Malentacca⁴⁷, A. Malinin⁴², T. Maltsev⁴², G. Manca^{30,l}, G. Mancinelli¹²,
C. Mancuso^{28,13,o}, R. Manera Escalero⁴⁴, D. Manuzzi²³, D. Marangotto^{28,o},
J.F. Marchand¹⁰, R. Marchevski⁴⁸, U. Marconi²³, E. Mariani¹⁵, S. Mariani⁴⁷,
C. Marin Benito⁴⁴, J. Marks²⁰, A.M. Marshall⁵³, L. Martel⁶², G. Martelli^{32,r},
G. Martellotti³⁴, L. Martinazzoli⁴⁷, M. Martinelli^{29,p}, D. Martinez Santos⁴⁵,
F. Martinez Vidal⁴⁶, A. Massafferri², R. Matev⁴⁷, A. Mathad⁴⁷, V. Matiunin⁴²,
C. Matteuzzi⁶⁷, K.R. Mattioli¹⁴, A. Mauri⁶⁰, E. Maurice¹⁴, J. Mauricio⁴⁴,
P. Mayencourt⁴⁸, J. Mazorra de Cos⁴⁶, M. Mazurek⁴⁰, M. McCann⁶⁰,
L. Mcconnell²¹, T.H. McGrath⁶¹, N.T. McHugh⁵⁸, A. McNab⁶¹, R. McNulty²¹,
B. Meadows⁶⁴, G. Meier¹⁸, D. Melnychuk⁴⁰, F. M. Meng^{4,c}, M. Merk^{36,77},
A. Merli⁴⁸, L. Meyer Garcia⁶⁵, D. Miao^{5,7}, H. Miao⁷, M. Mikhasenko⁷⁴,
D.A. Milanese⁷³, A. Minotti^{29,p}, E. Minucci⁶⁷, T. Miralles¹¹, B. Mitreska¹⁸,
D.S. Mitzel¹⁸, A. Modak⁵⁶, R.A. Mohammed⁶², R.D. Moise¹⁶, S. Mokhnenko⁴², E.
F. Molina Cardenas⁸¹, T. Mombächer⁴⁷, M. Monk^{55,1}, S. Monteil¹¹,
A. Morcillo Gomez⁴⁵, G. Morello²⁶, M.J. Morello^{33,s}, M.P. Morgenthaler²⁰,
A.B. Morris⁴⁷, A.G. Morris¹², R. Mountain⁶⁷, H. Mu^{4,c}, Z. M. Mu⁶,
E. Muhammad⁵⁵, F. Muheim⁵⁷, M. Mulder⁷⁶, K. Müller⁴⁹, F. Muñoz-Rojas⁹,
R. Murta⁶⁰, P. Naik⁵⁹, T. Nakada⁴⁸, R. Nandakumar⁵⁶, T. Namut⁴⁷, I. Nasteva³,
M. Needham⁵⁷, N. Neri^{28,o}, S. Neubert¹⁷, N. Neufeld⁴⁷, P. Neustroev⁴²,
J. Nicolini^{18,13}, D. Nicotra⁷⁷, E.M. Niel⁴⁸, N. Nikitin⁴², P. Nogarolli³,
P. Nogga¹⁷, N.S. Nolte⁶³, C. Normand⁵³, J. Novoa Fernandez⁴⁵, G. Nowak⁶⁴,
C. Nunez⁸¹, H. N. Nur⁵⁸, A. Oblakowska-Mucha³⁸, V. Obraztsov⁴², T. Oeser¹⁶,
S. Okamura^{24,m}, A. Okhotnikov⁴², O. Okhrimenko⁵¹, R. Oldeman^{30,l}, F. Oliva⁵⁷,
M. Olocco¹⁸, C.J.G. Onderwater⁷⁷, R.H. O'Neil⁵⁷, D. Osthues¹⁸,
J.M. Otalora Goicochea³, P. Owen⁴⁹, A. Oyanguren⁴⁶, O. Ozcelik⁵⁷, F. Paciolla^{33,w},

C. Trippel⁴³ , G. Tuci²⁰ , N. Tuning³⁶ , L.H. Uecker²⁰ , A. Ukleja³⁸ ,
D.J. Unverzagt²⁰ , E. Ursov⁴² , A. Usachov³⁷ , A. Ustyuzhanin⁴² , U. Uwer²⁰ ,
V. Vagnoni²³ , V. Valcarce Cadenas⁴⁵ , G. Valenti²³ , N. Valls Canudas⁴⁷ ,
H. Van Hecke⁶⁶ , E. van Herwijnen⁶⁰ , C.B. Van Hulse^{45,y} , R. Van Laak⁴⁸ ,
M. van Veghel³⁶ , G. Vasquez⁴⁹ , R. Vazquez Gomez⁴⁴ , P. Vazquez Regueiro⁴⁵ ,
C. Vázquez Sierra⁴⁵ , S. Vecchi²⁴ , J.J. Velthuis⁵³ , M. Veltri^{25,x} , A. Venkateswaran⁴⁸ ,
M. Vesterinen⁵⁵ , D. Vico Benet⁶² , P. Vidrier Villalba⁴⁴ , M. Vieites Diaz⁴⁷ ,
X. Vilasis-Cardona⁴³ , E. Vilella Figueras⁵⁹ , A. Villa²³ , P. Vincent¹⁵ , F.C. Volle⁵² ,
D. vom Bruch¹² , N. Voropaev⁴² , K. Vos⁷⁷ , G. Vouters^{10,47} , C. Vrahas⁵⁷ ,
J. Wagner¹⁸ , J. Walsh³³ , E.J. Walton^{1,55} , G. Wan⁶ , C. Wang²⁰ , G. Wang⁸ ,
J. Wang⁶ , J. Wang⁵ , J. Wang^{4,c} , J. Wang⁷² , M. Wang²⁸ , N. W. Wang⁷ ,
R. Wang⁵³ , X. Wang⁸ , X. Wang⁷⁰ , X. W. Wang⁶⁰ , Y. Wang⁶ , Z. Wang¹³ ,
Z. Wang^{4,c} , Z. Wang²⁸ , J.A. Ward^{55,1} , M. Waterlaet⁴⁷ , N.K. Watson⁵² ,
D. Websdale⁶⁰ , Y. Wei⁶ , J. Wendel⁷⁹ , B.D.C. Westhenry⁵³ , C. White⁵⁴ ,
M. Whitehead⁵⁸ , E. Whiter⁵² , A.R. Wiederhold⁶¹ , D. Wiedner¹⁸ , G. Wilkinson⁶² ,
M.K. Wilkinson⁶⁴ , M. Williams⁶³ , M.R.J. Williams⁵⁷ , R. Williams⁵⁴ , Z.
Williams⁵³ , F.F. Wilson⁵⁶ , W. Wislicki⁴⁰ , M. Witek³⁹ , L. Witola²⁰ ,
G. Wormser¹³ , S.A. Wotton⁵⁴ , H. Wu⁶⁷ , J. Wu⁸ , Y. Wu⁶ , Z. Wu⁷ ,
K. Wyllie⁴⁷ , S. Xian⁷⁰ , Z. Xiang⁵ , Y. Xie⁸ , A. Xu³³ , J. Xu⁷ , L. Xu^{4,c} ,
L. Xu^{4,c} , M. Xu⁵⁵ , Z. Xu⁴⁷ , Z. Xu⁷ , Z. Xu⁵ , D. Yang⁴ , K. Yang⁶⁰ ,
S. Yang⁷ , X. Yang⁶ , Y. Yang^{27,n} , Z. Yang⁶ , Z. Yang⁶⁵ , V. Yeroshenko¹³ ,
H. Yeung⁶¹ , H. Yin⁸ , X. Yin⁷ , C. Y. Yu⁶ , J. Yu⁶⁹ , X. Yuan⁵ , Y. Yuan^{5,7} ,
E. Zaffaroni⁴⁸ , M. Zavertyaev¹⁹ , M. Zdybal³⁹ , F. Zenesini^{23,k} , C. Zeng^{5,7} ,
M. Zeng^{4,c} , C. Zhang⁶ , D. Zhang⁸ , J. Zhang⁷ , L. Zhang^{4,c} , S. Zhang⁶⁹ ,
S. Zhang⁶² , Y. Zhang⁶ , Y. Z. Zhang^{4,c} , Y. Zhao²⁰ , A. Zharkova⁴² ,
A. Zhelezov²⁰ , S. Z. Zheng⁶ , X. Z. Zheng^{4,c} , Y. Zheng⁷ , T. Zhou⁶ , X. Zhou⁸ ,
Y. Zhou⁷ , V. Zhovkovska⁵⁵ , L. Z. Zhu⁷ , X. Zhu^{4,c} , X. Zhu⁸ , V. Zhukov¹⁶ ,
J. Zhuo⁴⁶ , Q. Zou^{5,7} , D. Zuliani^{31,q} , G. Zunica⁴⁸ .

¹*School of Physics and Astronomy, Monash University, Melbourne, Australia*

²*Centro Brasileiro de Pesquisas Físicas (CBPF), Rio de Janeiro, Brazil*

³*Universidade Federal do Rio de Janeiro (UFRJ), Rio de Janeiro, Brazil*

⁴*Department of Engineering Physics, Tsinghua University, Beijing, China, Beijing, China*

⁵*Institute Of High Energy Physics (IHEP), Beijing, China*

⁶*School of Physics State Key Laboratory of Nuclear Physics and Technology, Peking University, Beijing, China*

⁷*University of Chinese Academy of Sciences, Beijing, China*

⁸*Institute of Particle Physics, Central China Normal University, Wuhan, Hubei, China*

⁹*Consejo Nacional de Rectores (CONARE), San Jose, Costa Rica*

¹⁰*Université Savoie Mont Blanc, CNRS, IN2P3-LAPP, Annecy, France*

¹¹*Université Clermont Auvergne, CNRS/IN2P3, LPC, Clermont-Ferrand, France*

¹²*Aix Marseille Univ, CNRS/IN2P3, CPPM, Marseille, France*

¹³*Université Paris-Saclay, CNRS/IN2P3, IJCLab, Orsay, France*

¹⁴*Laboratoire Leprince-Ringuet, CNRS/IN2P3, Ecole Polytechnique, Institut Polytechnique de Paris, Palaiseau, France*

¹⁵*LPNHE, Sorbonne Université, Paris Diderot Sorbonne Paris Cité, CNRS/IN2P3, Paris, France*

¹⁶*I. Physikalisches Institut, RWTH Aachen University, Aachen, Germany*

¹⁷*Universität Bonn - Helmholtz-Institut für Strahlen und Kernphysik, Bonn, Germany*

¹⁸*Fakultät Physik, Technische Universität Dortmund, Dortmund, Germany*

¹⁹*Max-Planck-Institut für Kernphysik (MPIK), Heidelberg, Germany*

²⁰*Physikalisches Institut, Ruprecht-Karls-Universität Heidelberg, Heidelberg, Germany*

²¹*School of Physics, University College Dublin, Dublin, Ireland*

²²*INFN Sezione di Bari, Bari, Italy*

- ²³ INFN Sezione di Bologna, Bologna, Italy
- ²⁴ INFN Sezione di Ferrara, Ferrara, Italy
- ²⁵ INFN Sezione di Firenze, Firenze, Italy
- ²⁶ INFN Laboratori Nazionali di Frascati, Frascati, Italy
- ²⁷ INFN Sezione di Genova, Genova, Italy
- ²⁸ INFN Sezione di Milano, Milano, Italy
- ²⁹ INFN Sezione di Milano-Bicocca, Milano, Italy
- ³⁰ INFN Sezione di Cagliari, Monserrato, Italy
- ³¹ INFN Sezione di Padova, Padova, Italy
- ³² INFN Sezione di Perugia, Perugia, Italy
- ³³ INFN Sezione di Pisa, Pisa, Italy
- ³⁴ INFN Sezione di Roma La Sapienza, Roma, Italy
- ³⁵ INFN Sezione di Roma Tor Vergata, Roma, Italy
- ³⁶ Nikhef National Institute for Subatomic Physics, Amsterdam, Netherlands
- ³⁷ Nikhef National Institute for Subatomic Physics and VU University Amsterdam, Amsterdam, Netherlands
- ³⁸ AGH - University of Krakow, Faculty of Physics and Applied Computer Science, Kraków, Poland
- ³⁹ Henryk Niewodniczanski Institute of Nuclear Physics Polish Academy of Sciences, Kraków, Poland
- ⁴⁰ National Center for Nuclear Research (NCBJ), Warsaw, Poland
- ⁴¹ Horia Hulubei National Institute of Physics and Nuclear Engineering, Bucharest-Magurele, Romania
- ⁴² Affiliated with an institute covered by a cooperation agreement with CERN
- ⁴³ DS4DS, La Salle, Universitat Ramon Llull, Barcelona, Spain
- ⁴⁴ ICCUB, Universitat de Barcelona, Barcelona, Spain
- ⁴⁵ Instituto Galego de Física de Altas Enerxías (IGFAE), Universidade de Santiago de Compostela, Santiago de Compostela, Spain
- ⁴⁶ Instituto de Física Corpuscular, Centro Mixto Universidad de Valencia - CSIC, Valencia, Spain
- ⁴⁷ European Organization for Nuclear Research (CERN), Geneva, Switzerland
- ⁴⁸ Institute of Physics, Ecole Polytechnique Fédérale de Lausanne (EPFL), Lausanne, Switzerland
- ⁴⁹ Physik-Institut, Universität Zürich, Zürich, Switzerland
- ⁵⁰ NSC Kharkiv Institute of Physics and Technology (NSC KIPT), Kharkiv, Ukraine
- ⁵¹ Institute for Nuclear Research of the National Academy of Sciences (KINR), Kyiv, Ukraine
- ⁵² School of Physics and Astronomy, University of Birmingham, Birmingham, United Kingdom
- ⁵³ H.H. Wills Physics Laboratory, University of Bristol, Bristol, United Kingdom
- ⁵⁴ Cavendish Laboratory, University of Cambridge, Cambridge, United Kingdom
- ⁵⁵ Department of Physics, University of Warwick, Coventry, United Kingdom
- ⁵⁶ STFC Rutherford Appleton Laboratory, Didcot, United Kingdom
- ⁵⁷ School of Physics and Astronomy, University of Edinburgh, Edinburgh, United Kingdom
- ⁵⁸ School of Physics and Astronomy, University of Glasgow, Glasgow, United Kingdom
- ⁵⁹ Oliver Lodge Laboratory, University of Liverpool, Liverpool, United Kingdom
- ⁶⁰ Imperial College London, London, United Kingdom
- ⁶¹ Department of Physics and Astronomy, University of Manchester, Manchester, United Kingdom
- ⁶² Department of Physics, University of Oxford, Oxford, United Kingdom
- ⁶³ Massachusetts Institute of Technology, Cambridge, MA, United States
- ⁶⁴ University of Cincinnati, Cincinnati, OH, United States
- ⁶⁵ University of Maryland, College Park, MD, United States
- ⁶⁶ Los Alamos National Laboratory (LANL), Los Alamos, NM, United States
- ⁶⁷ Syracuse University, Syracuse, NY, United States
- ⁶⁸ Pontifícia Universidade Católica do Rio de Janeiro (PUC-Rio), Rio de Janeiro, Brazil, associated to ³
- ⁶⁹ School of Physics and Electronics, Hunan University, Changsha City, China, associated to ⁸
- ⁷⁰ Guangdong Provincial Key Laboratory of Nuclear Science, Guangdong-Hong Kong Joint Laboratory of Quantum Matter, Institute of Quantum Matter, South China Normal University, Guangzhou, China, associated to ⁴
- ⁷¹ Lanzhou University, Lanzhou, China, associated to ⁵
- ⁷² School of Physics and Technology, Wuhan University, Wuhan, China, associated to ⁴
- ⁷³ Departamento de Física, Universidad Nacional de Colombia, Bogota, Colombia, associated to ¹⁵
- ⁷⁴ Ruhr Universitaet Bochum, Fakultae f. Physik und Astronomie, Bochum, Germany, associated to ¹⁸

- ⁷⁵ *Eotvos Lorand University, Budapest, Hungary, associated to* ⁴⁷
⁷⁶ *Van Swinderen Institute, University of Groningen, Groningen, Netherlands, associated to* ³⁶
⁷⁷ *Universiteit Maastricht, Maastricht, Netherlands, associated to* ³⁶
⁷⁸ *Tadeusz Kosciuszko Cracow University of Technology, Cracow, Poland, associated to* ³⁹
⁷⁹ *Universidade da Coruña, A Coruña, Spain, associated to* ⁴³
⁸⁰ *Department of Physics and Astronomy, Uppsala University, Uppsala, Sweden, associated to* ⁵⁸
⁸¹ *University of Michigan, Ann Arbor, MI, United States, associated to* ⁶⁷
⁸² *Université Paris-Saclay, Centre d'Etudes de Saclay (CEA), IRFU, Saclay, France, Gif-Sur-Yvette, France*

^a *Universidade de Brasília, Brasília, Brazil*

^b *Centro Federal de Educação Tecnológica Celso Suckow da Fonseca, Rio De Janeiro, Brazil*

^c *Center for High Energy Physics, Tsinghua University, Beijing, China*

^d *Hangzhou Institute for Advanced Study, UCAS, Hangzhou, China*

^e *School of Physics and Electronics, Henan University, Kaifeng, China*

^f *LIP6, Sorbonne Université, Paris, France*

^g *Lamarr Institute for Machine Learning and Artificial Intelligence, Dortmund, Germany*

^h *Universidad Nacional Autónoma de Honduras, Tegucigalpa, Honduras*

ⁱ *Università di Bari, Bari, Italy*

^j *Università di Bergamo, Bergamo, Italy*

^k *Università di Bologna, Bologna, Italy*

^l *Università di Cagliari, Cagliari, Italy*

^m *Università di Ferrara, Ferrara, Italy*

ⁿ *Università di Genova, Genova, Italy*

^o *Università degli Studi di Milano, Milano, Italy*

^p *Università degli Studi di Milano-Bicocca, Milano, Italy*

^q *Università di Padova, Padova, Italy*

^r *Università di Perugia, Perugia, Italy*

^s *Scuola Normale Superiore, Pisa, Italy*

^t *Università di Pisa, Pisa, Italy*

^u *Università della Basilicata, Potenza, Italy*

^v *Università di Roma Tor Vergata, Roma, Italy*

^w *Università di Siena, Siena, Italy*

^x *Università di Urbino, Urbino, Italy*

^y *Universidad de Alcalá, Alcalá de Henares, Spain*

^z *Facultad de Ciencias Físicas, Madrid, Spain*

^{aa} *Department of Physics/Division of Particle Physics, Lund, Sweden*

[†] *Deceased*